Description of Response of Materials to Pulsed Thermonuclear Radiation - Part III: Response Modification by Intermediate Gaseous Layers

T.O. Hunter and G.L. Kulcinski

April 1977

UWFDM-232

FUSION TECHNOLOGY INSTITUTE

UNIVERSITY OF WISCONSIN

MADISON WISCONSIN

Description of Response of Materials to Pulsed Thermonuclear Radiation - Part III: Response Modification by Intermediate Gaseous Layers

T.O. Hunter and G.L. Kulcinski

Fusion Technology Institute
University of Wisconsin
1500 Engineering Drive
Madison, WI 53706

http://fti.neep.wisc.edu

April 1977

UWFDM-232

Description of the Response of Materials to Pulsed Thermonuclear Radiation

(Part III)

Effect of Gases on Modification of Pellet Debris Spectra and First Wall Response

Thomas O. Hunter*

G.L. Kulcinski

April 1978

Fusion Research Program
University of Wisconsin
Madison, Wisconsin 53706

UWFDM-232

*Member Technical Staff, Sandia Laboratories, Albuquerque, NM 87115. Work partially supported by the U.S. Department of Energy.

Table of Contents

I. Introduction

This document is the third in a series[1,2] which provides the basis of a general model for analysis of the radiation damage environment from transient thermonuclear radiation. Part I outlined the systematic approach to be followed and gave some theoretical basis for the interaction of pulsed radiation with materials. Part II presented models for the transient energy deposition, temperatures, and displacement rates. In this segment, some related extensions of these models are presented; first of all, models for analyzing the role of gas protection in modifying the spectra are derived and then these models are used to predict the alteration of surface temperature with the introduction of various gases.

II. Role of Gas Protection

Survival of first walls and other components in inertial confinement fusion systems may require the use of protective systems to reduce the energy flux of ions and photons which are part of the fusion microexplosion. Numerous methods have been proposed previously which include magnetic fields,[3] liquid walls,[4] and gas layers.[5] This chapter will investigate the latter of these methods and will consider two aspects: 1) the data for the stopping of ions in gases, and 2) a general model for determining the modification of ion spectra while transiting gases.

Inherent in all the subsequent discussions is that, as a first approximation, the ion spectra from a pellet microexplosion can be considered as fully developed into directed kinetic energy at radial distances large compared to the pellet but small compared to the wall radius or position

of an exposed component. In addition, the slowing down characteristics of ions in rarefied gases is assumed to be the same as in any homogeneous isotropic material except for the proportionality to atom density. As an aid to the reader we have included in this section, calculations of the range of various ions from fusion microexplosions in two gases which are considered candidates for gaseous protection: neon and xenon.

The range and straggling data are obtained from calculations performed on the COREL code by Brice[6] and incorporate electronic stopping powers based on the 3 parameter formulation discussed in Part I.[1] In all cases the nuclear cross sections are based on the theory of Lindhard,[7] et al. Calculations were performed for the following ions and energy ranges.

Deuterium	0 - 1000 keV
Tritium	0 - 1400 keV
Helium	0 - 4000 keV
Silicon	0 - 10,000 keV
Mercury	0 - 10,000 keV

All data are normalized to a pressure of 1 Torr at standard temperature which corresponds to an atom density of 3.54×10^{16} atoms/cm^3.

Figures 1-5 display the results for both the range calculations and the range plus or minus two standard deviations ($\pm 2\sigma$).

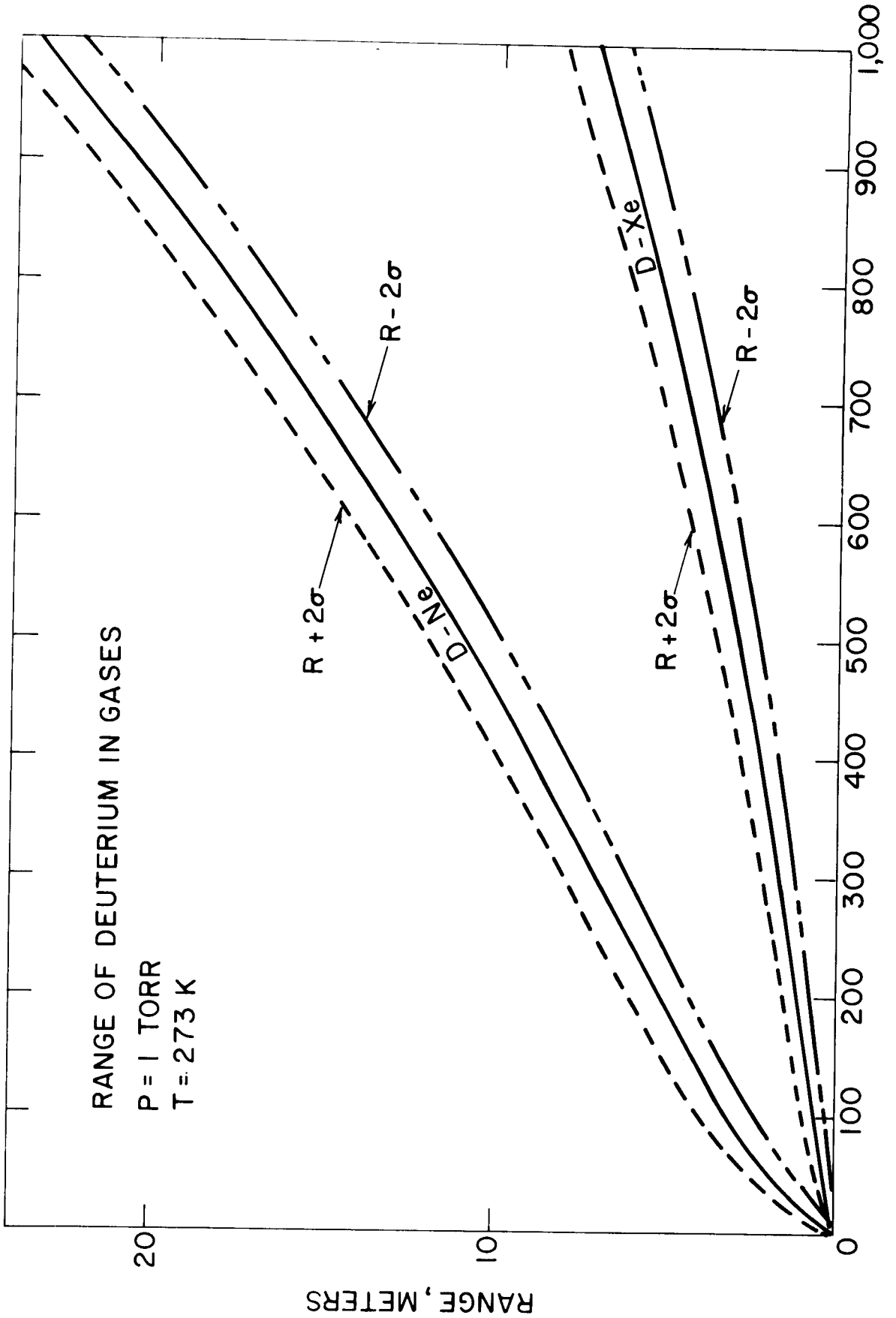
RANGE OF DEUTERIUM IN GASES
P = 1 TORR
T = 273 K
D-Ne
D-Xe
R + 2σ
R - 2σ
R + 2σ
R - 2σ
RANGE, METERS
ENERGY, KeV
0
10
20
100
200
300
400
500
600
700
800
900
1,000

FIGURE 1

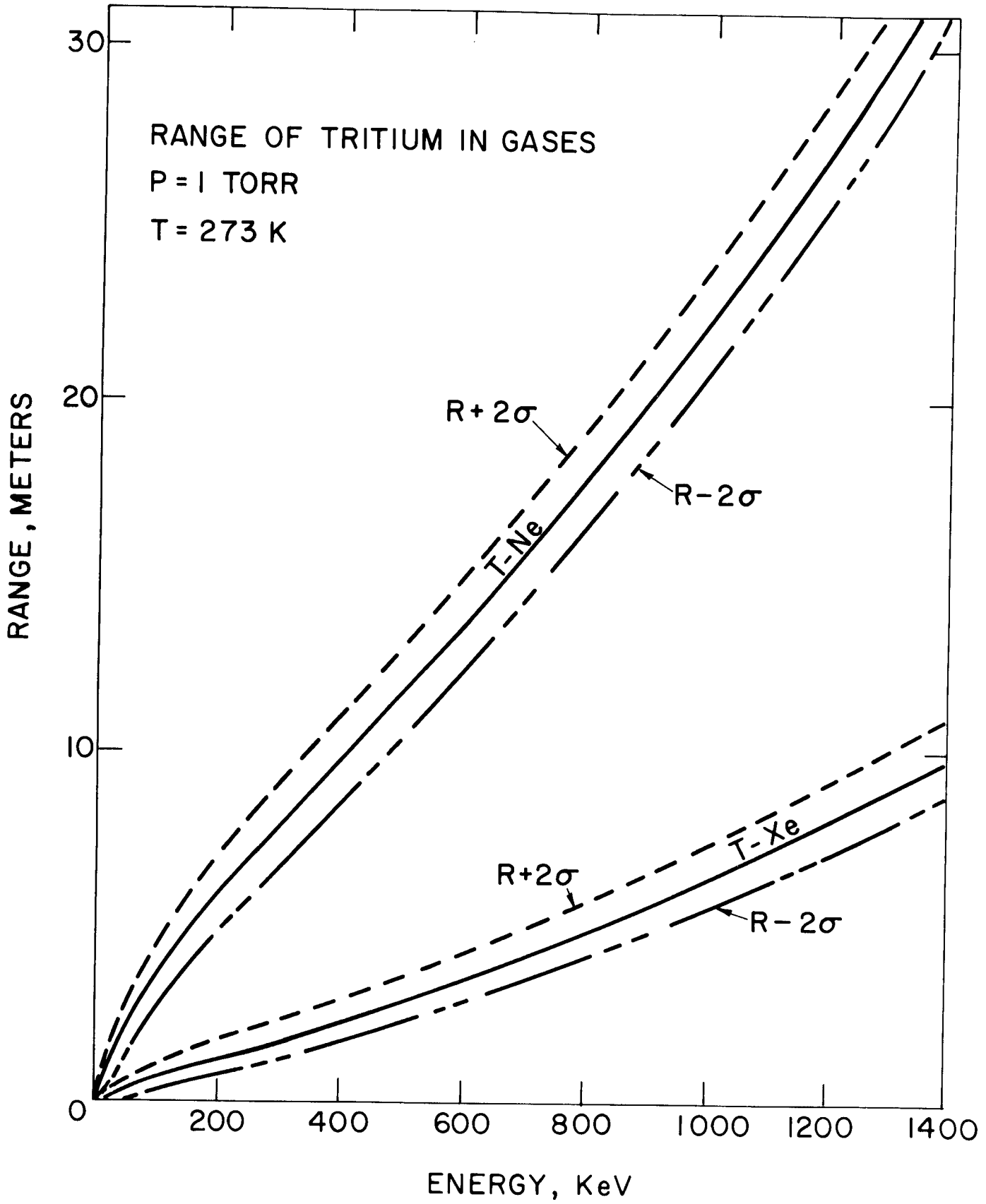
RANGE OF TRITIUM IN GASES
P = 1 TORR
T = 273 K
R+2σ
R-2σ
T-Ne
T-Xe
R+2σ
R-2σ
RANGE, METERS
ENERGY, KeV
0
10
20
30
200
400
600
800
1000
1200
1400

FIGURE 2

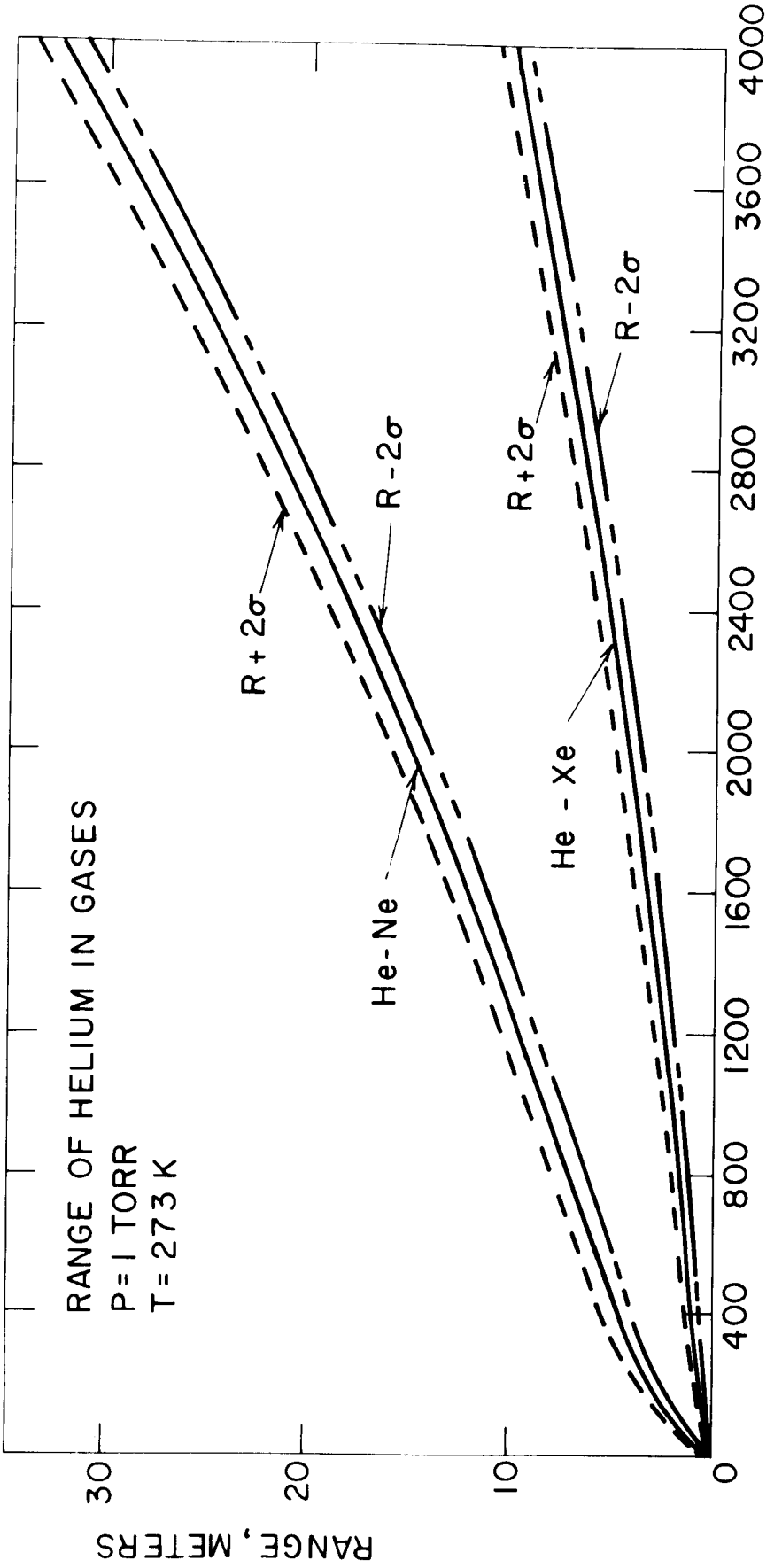
RANGE OF HELIUM IN GASES
P = 1 TORR
T = 273 K
He-Ne
He - Xe
R + 2σ
R - 2σ
R + 2σ
R - 2σ
RANGE, METERS
ENERGY, KeV
0
10
20
30
400
800
1200
1600
2000
2400
2800
3200
3600
4000

FIGURE 3

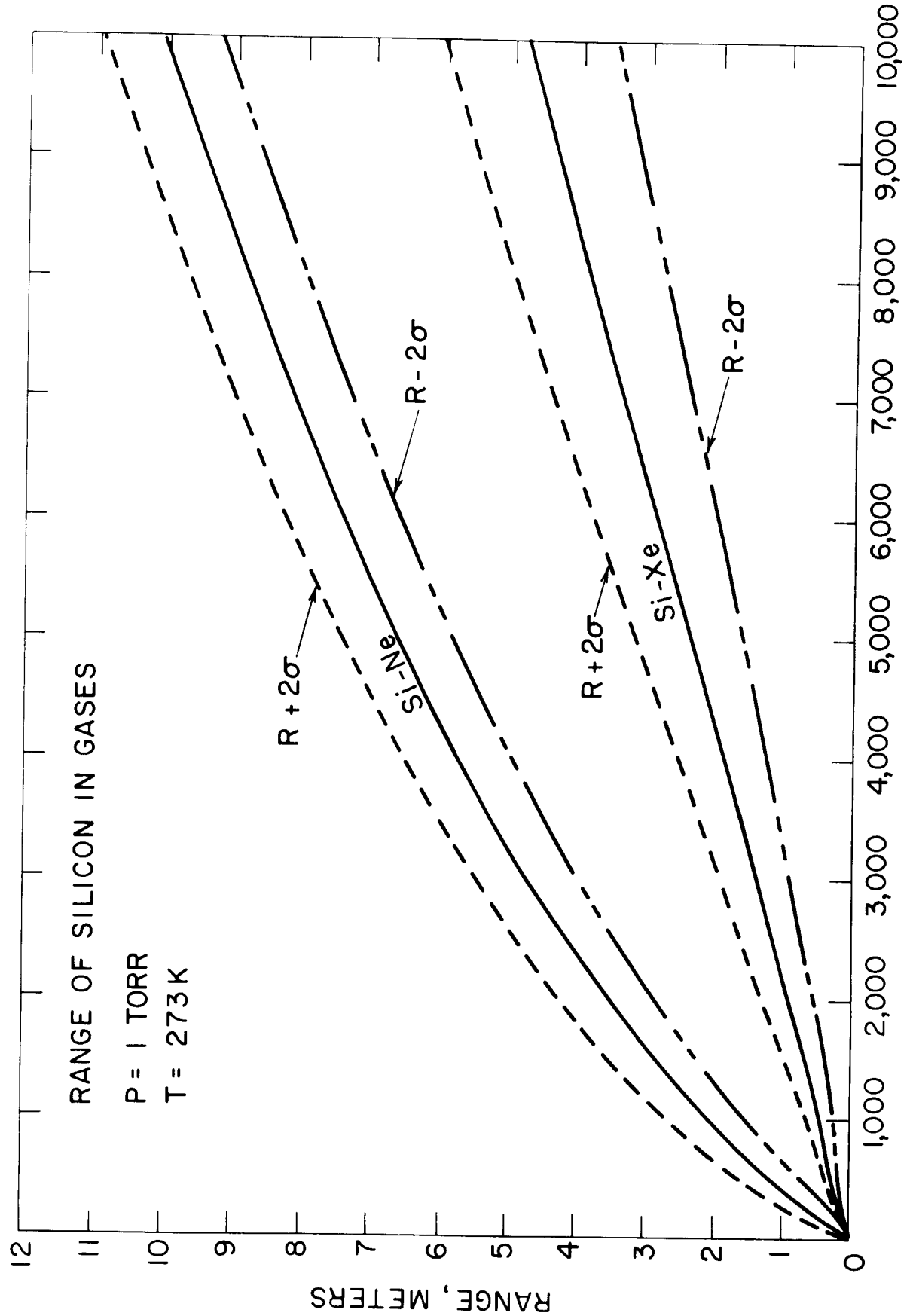
RANGE OF SILICON IN GASES
P = 1 TORR
T = 273 K
Si-Ne
Si-Xe
R + 2σ
R - 2σ
R + 2σ
R - 2σ
RANGE, METERS
ENERGY, KeV
0
1
2
3
4
5
6
7
8
9
10
11
12
1,000
2,000
3,000
4,000
5,000
6,000
7,000
8,000
9,000
10,000

FIGURE 4

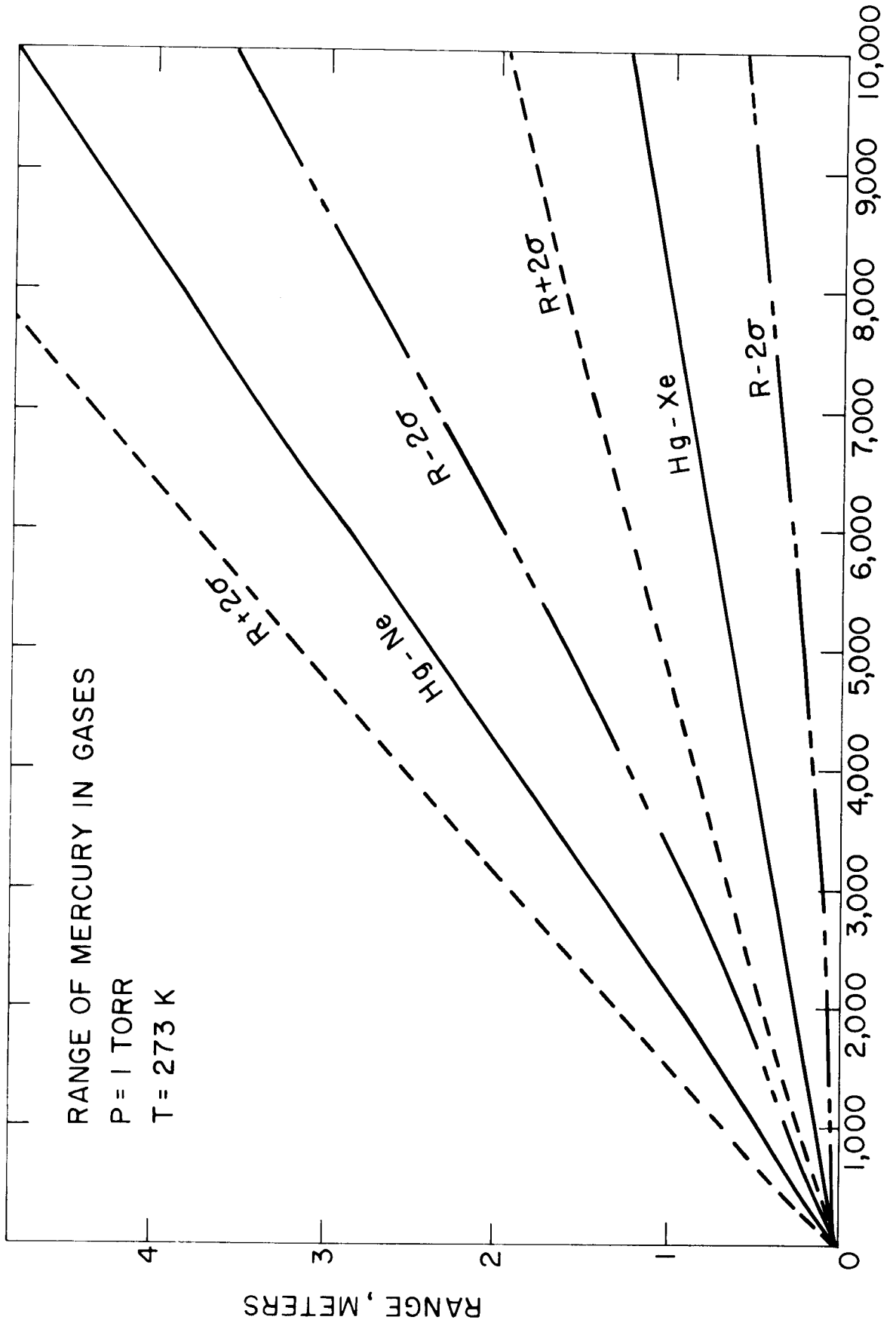
RANGE OF MERCURY IN GASES
P = 1 TORR
T = 273 K
Hg-Ne
R+2σ
R-2σ
R+2σ
Hg-Xe
R-2σ
RANGE, METERS
0
1
2
3
4
1,000
2,000
3,000
4,000
5,000
6,000
7,000
8,000
9,000
10,000
ENERGY, KeV

FIGURE 5

III. Modification of Ion Spectra in Gases

In this section a general method will be developed which can be used to estimate the modification of the energy spectra of the ions as they proceed through a material. This method will first be developed for a monoenergetic spectrum and then generalized for an arbitrary spectrum. Separate treatments are used for heavy ions (or low energy light ions) and light ions of higher energy. The former is based on a diffusion approximation to the transport of ions where the distributions for monoenergetic ions must consider more than one moment. The light ion method will be based on the stopping power functions given in Part II.[2]

III.A. Diffusion Approximation to Ion Transport in Materials

The penetration and distribution of ions in materials can be rigorously solved by obtaining a solution of the transport equation accounting for the interaction of the ions with the electrons and nuclei in the material. In this development a simple treatment will be given which will allow an approximate determination of the spatial distribution of ions at various times between impact and stopping. This information can then be used to determine the flux and spectrum of the ions at any position within the materials.

Various treatments are available to evaluate the moments of the final ion distribution, i.e., when the ion comes to rest. The methods of Gibbons and Johnson,[8] Winterbon,[9] and Brice[10] are examples. Brice also presents a direct method for determining the first and second central moments of the distribution at intermediate energies. These data have been used by Tsurushima and Tanoue[11] to determine the ion spectra at a specified position in the material.

Unfortunately, Brice's method requires an appreciable amount of computation using the RASE4[6] code even if only a few incident energies are examined. If a large number of incident energies (e.g., typical of the debris spectra from a TN pellet burn) are examined, the computation can become quite expensive. Consequently this, and the method of Tsurushima and Tanoue are not considered appropriate when as many as 5 to 8 different ions, each with broad energy spectra, are considered for one pellet design.

All the previous treatments incorporate the nuclear cross sections and ion-electron interactions and solve for the moments of the ion distributions with an expansion solution. The approach taken in this paper will assume that the first and second moments of the final ion distribution are available. These may be obtained for any ion-target combination by any of the above formulations. Specifically, values may be taken from the codes of Manning and Mueller[12] or the COREL code of Brice.[6] However, caution should be used in choosing between the two codes, because although they both agree on the first moments (ranges), they can have substantially different second moments (ΔR). The COREL code gives the more accurate values for the straggling and is thus recommended.

III.A.1. Monoenergetic Solutions

When an ion of incident energy E_* passes through a finite density of target atoms and comes to rest, the probability of finding it anywhere around the projected range will have a gaussian shape with a mean R and standard deviation σ. As stated above it is assumed this represents the distribution when the energy is zero and that R (range) and σ (ΔR) are well-known. In addition, it is assumed that this distribution is reached when the time after impact has some finite value, t_o.

The gaussian distribution of implanted particles can be assumed to be the result of two processes:

1) A general slowing down which determines the position of the mean of the distribution, and

2) A diffusive process which determines the spread or second central moment.

The latter assumption is analogous to the diffusion of neutrons produced by their scattering interactions with the host atoms.

The initial conditions are established by the assertion that at impact the distribution is centered at the origin (x = 0) and has no spatial or spectral variance. A solution will now be developed which satisfies the initial and final values as boundary conditions, and which can then be used to approximate the distribution anywhere in between. The ion distribution is assumed to be "diffusing" about the center-of-mass or the mean of the distribution. It is also assumed that the motion of the center-of-mass can be determined from the range-energy relationship for the ion-target combination considered.

III.A.1.a. Diffusion in Center-of-Mass

Consider a solution for the concentration of ions in the "center-of-mass" (COM) reference frame. At time = 0 (impact), the distribution is a delta function in space centered at r = 0. If x is the spatial variable in the COM frame, then the diffusion equation is

$$\frac{\partial^2 c}{\partial x^2} - \frac{1}{\gamma^2}\frac{\partial c}{\partial t} = C_o\,\delta(x)\,\delta(t) \qquad (1)$$

where c is the concentration of ions per unit volume at time t and position x,

γ is a diffusion coefficient as yet undetermined, and

$$\int_t C_o \, \delta(t) \, dt = F$$

where F is the incident fluence, ions/cm^2.

The solution to 1) is well-known as[13]

$$c(x,t) = \frac{C_o}{(4\pi\gamma^2 t)^{\frac{1}{2}}} \exp\left(-\frac{x^2}{4\gamma^2 t}\right) \tag{2}$$

The effect of the nuclear interaction contribution to the scattering is contained in the term γ. This term would be difficult to obtain from first principles; however, we can determine an estimate of its value from the knowledge of its effect on the final distribution. This is given by the gaussian approximation as:

$$c(x,t_o) = \frac{C_o}{(2\pi)^{\frac{1}{2}}\sigma} \exp\left(-x^2/2\sigma^2\right) \tag{3}$$

Thus an estimate for γ is

$$\gamma = \sigma/\sqrt{2t_o}$$

where t_o is the time when E = 0.

III.A.1.b. Motion of Center-of-Mass

In addition to the diffusion in the center-of-mass it is necessary to determine motion of the center-of-mass. If it is assumed that motion of the COM is independent of the dispersion of the distribution, the equation of motion can be solved directly.

In general, it will be assumed that the range energy relationship can be expressed in the following functional form:

$$R = C\, V_*^{\frac{1}{1-k}} \tag{4}$$

where R = range (position when $V = E = 0$)

V_* = incident velocity,

and C, k are constants determined from range-energy data.

In addition it is assumed that

$$\frac{dr}{dV} = \frac{dR}{dV_*} \tag{5}$$

where r is the position of the COM (in the lab system) at any time,

V is the velocity of the COM at any time.

The position is then given by

$$r = \int_o^r dr = - \int_{V_*}^{V} \frac{dr}{dV}\, dV$$

$$r = C\, V^{\frac{1}{1-k}} \Bigg|_{V}^{V_*}$$

or

$$r = C \left\{V_*^{\frac{1}{1-k}} - V^{\frac{1}{1-k}}\right\} \tag{6}$$

The form of equation 4 was chosen because it closely resembles the stopping of heavy ions in materials. The case of $k = \frac{1}{2}$ ($R = CV^2$) corresponds to a uniform spatial energy deposition over the range of the ion which is characteristic of low velocity ions when nuclear and electronic stopping powers are equivalent.

The case of k = 0 (R = CV) corresponds to a deposition relationship of

$$\frac{dE}{dx} \propto E^{\frac{1}{2}}$$

which is the anticipated form for an interaction which is electronic dominated with the form of the stopping taken from Lindhard theory.[7]

Values of k and C may be easily determined if two data points are known for the ion-target combination. Hence, given V_{*1}, R_1 and V_{*2}, R_2, the following simple conditions yield the constants.

$$k = 1 - \frac{\ell n\ V_{*1}/V_{*2}}{\ell n\ R_1/R_2}$$

$$C = \frac{R_1}{(V_{*1})^{1/(1-k)}}$$

The standard deviation at the end-of-range can be expressed as

$$\tilde{\sigma}\ (V_*) = F(V_*)R(V_*) \qquad (7)$$

where $F(V_*)$ has been assumed for this study to be:

$$F(V_*) = A \exp\ (-V_*/B)$$

and from two data points

$$B = \frac{(V_2 - V_1)}{\ell n(\frac{\tilde{\sigma}_1 R_2}{\tilde{\sigma}_2 R_1})}$$

$$A = (\tilde{\sigma}_1/R_1) \exp\ (V_1/B)$$

Equations 4 and 7 allow the determination of the normal range and standard deviation in normal range when the ion has come to rest for any incident energy ion.

The time for an ion of incident energy E_* or velocity V_* to reach a position r between 0 and R is

$$t = \int_o^r \frac{dr}{V} = \int_o^r \frac{dr}{(V_*^{\frac{1}{1-k}} - r/C)^{1-k}} \qquad \text{for } r < R \tag{8}$$

which has the result

$$t = \frac{C}{k} \{V_*^{k/1-k} - (V_*^{\frac{1}{1-k}} - r/C)^k\} \tag{9}$$

in terms of velocity equation 9 can be written

$$t = \frac{C}{k} \{V_*^{k/1-k} - V^{k/1-k}\} . \tag{10}$$

Equation 9 can also be rewritten for more accurate numerical evaluation as:

$$t = \frac{C}{k} V_*^{\frac{k}{1-k}} \{1 - (1-\frac{r}{C} V_*^{\frac{1}{k-1}})^k\} . \tag{11}$$

The inverse functions to equations 9 to 10 can be used to evaluate the position of the mean at a given time and the velocity at a given time as:

$$r = CV_*^{\frac{1}{1-k}} \{1-(1-\frac{tk}{C} V_*^{\frac{k}{k-1}})^{1/k}\} \tag{12}$$

and

$$V = \{V_*^{\frac{k}{1-k}} - \frac{tk}{C}\}^{\frac{1-k}{k}} \tag{13}$$

III.A.1.c. General Solution

The results can now be superimposed combining the center-of-mass motion and the "diffusion" of the distribution. The distribution at any time would be given as

$$c(x,t) = \frac{C_o}{(4\pi\gamma^2 t)^{\frac{1}{2}}} \exp - \frac{(r(t)-x)^2}{4\gamma^2 t} \tag{14}$$

where r(t) is given by equation (12) at time t

x is any position within the material where the distribution is desired. The distribution at any intermediate velocity is

$$c(x,V) = \frac{C_o}{(4\pi\gamma^2 t(V))^{\frac{1}{2}}} \exp - \frac{(r(V)-x)^2}{4\gamma^2 t(V)} \tag{15}$$

where t(V) = equation 10

r(V) = equation 6

The previous relations allow an estimate of the position of the mean and of the standard deviation of the ion distribution at any time or intermediate energy between impact and stopping. These results, therefore, represent a simple method for determining the same results as the Brice analysis in the RASE4 code.[6] The relations here clearly do not maintain the accuracy or the elegance of Brice's solution but they can allow approximate determination of the distributions with a relatively small amount of numerical calculation. These results will now be used to evaluate the normal flux and spectra passing through any intermediate position.

III.A.1.d. Flux and Spectra at Arbitrary Position

The instantaneous flux of particles passing through any position can be determined as the product of the concentration and the normal velocity as

$$F(t,x) = c(t,x)\ V(t,x) \tag{16}$$

Since the velocity is the same for each ion in any given gaussian distribution, the flux can be evaluated as:

$$F(t,x) = \frac{C_o}{(4\pi\gamma^2 t)^{\frac{1}{2}}} \exp - \frac{(r(t)-x)^2}{4\gamma^2 t} \quad \{V_*^{\frac{k}{1-k}} - \frac{tk}{C}\}^{\frac{1-k}{k}} \tag{17}$$

$$= \text{eqn 14 x eqn 13}$$

The velocity spectrum can be determined as

$$G(V,x) = - F(t,x) \frac{dt}{dV} \tag{18}$$

which by differentiating equation 10

$$G(V,x) = F(t,x) \frac{C}{1-k} V^{\frac{2k-1}{1-k}} \tag{19}$$

The energy spectrum is given by

$$S(E,x) = G(V,x) \frac{dV}{dE} \tag{20}$$

$$\text{Since } V = [4.39 \times 10^7] (E/m)^{\frac{1}{2}} \tag{21}$$

where E = keV

m = amu

V = cm/sec

$$\text{then, } S(E,x) = [2.20 \times 10^7] G(V,x)/(mE)^{\frac{1}{2}} \tag{22}$$

Equations 17, 19 and 22 are the functions which can be used for evaluation of the flux and spectra at any intermediate position or time.

To this point, the discussion has pertained only to monoenergetic incident ions and must now be generalized to the case where the incident spectrum is considered. Before addressing the case of an arbitrary spectrum we make a comparison of the results of the above analysis with the same analysis using the RASE4 code for Ni ions passing through nickel (figure 6).

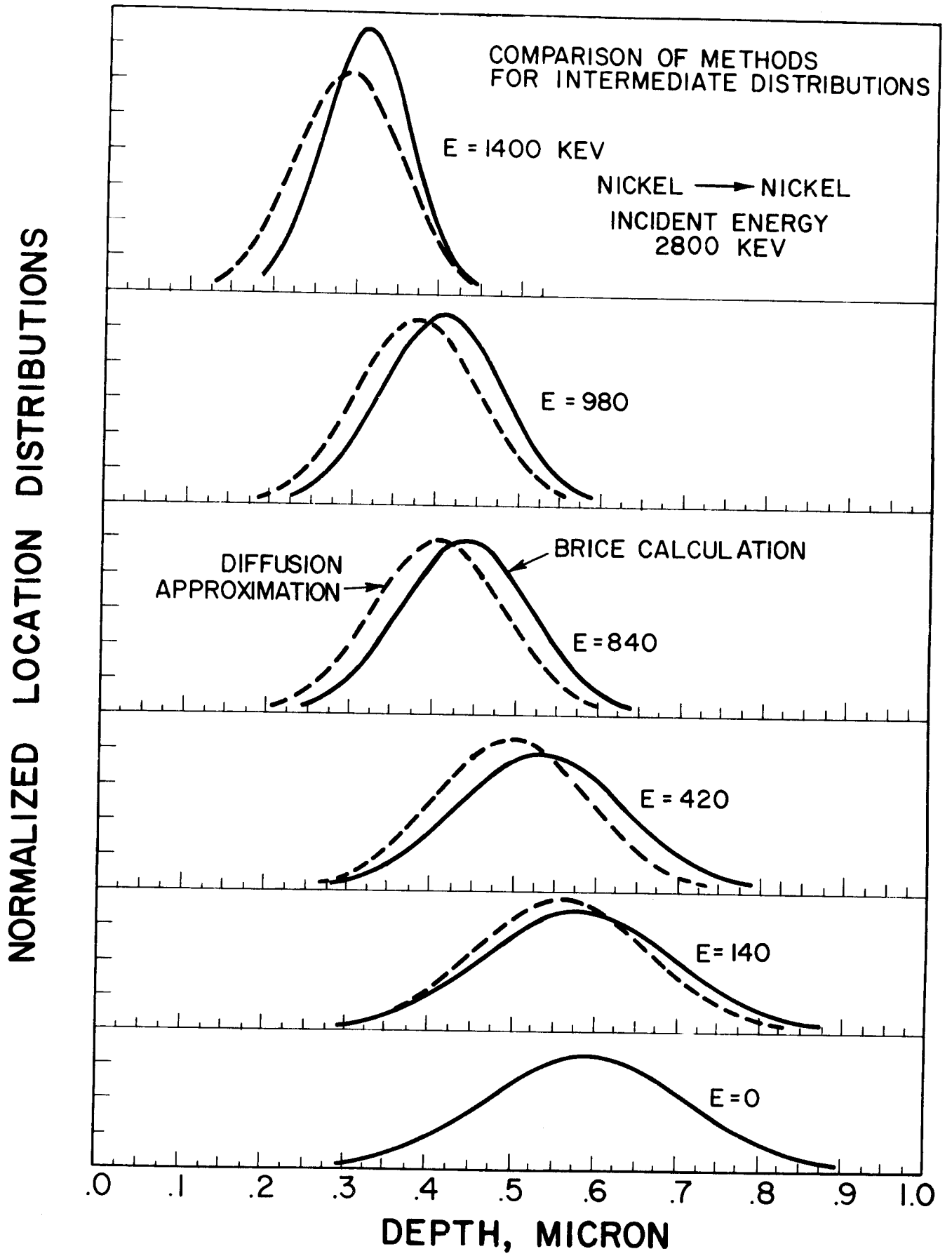
COMPARISON OF METHODS
FOR INTERMEDIATE DISTRIBUTIONS
E = 1400 KEV
NICKEL → NICKEL
INCIDENT ENERGY
2800 KEV
E = 980
DIFFUSION
APPROXIMATION
BRICE CALCULATION
E = 840
E = 420
E = 140
E = 0
NORMALIZED LOCATION DISTRIBUTIONS
.0
.1
.2
.3
.4
.5
.6
.7
.8
.9
1.0
DEPTH, MICRON

FIGURE 6

The agreement, although not precise, is sufficiently close considering the inherent accuracy of any ion implantation theoretical analysis. The principal advantage of the technique derived in this paper is that it can be applied in a rather inexpensive calculation of a large number of incident ions.

III.A.2. Application to an Incident Spectrum

If the incident spectrum is not monoenergetic, it is necessary to determine the spectra and temporal characteristics of all the ions as they pass through the material.

The incident spectrum is described at time = 0 in figure 7.

FIGURE 7

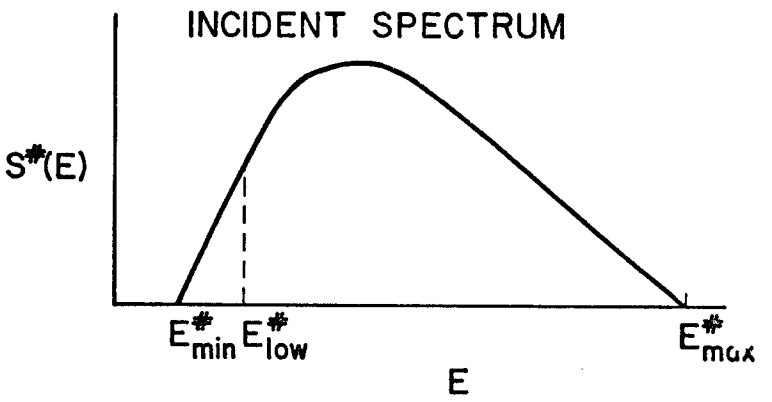

where S*(E) is an arbitrary function.

If this spectrum is to pass through a buffer material in which its form will be modified, it is necessary to evaluate the modified flux and spectra at some position, Z, with the material.

At position Z the ion flux will take the form F(t,Z) as figure 8:

FIGURE 8

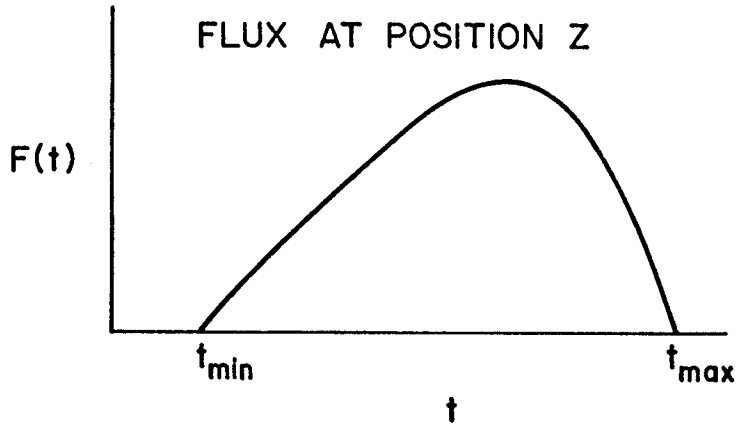

To evaluate this distribution for finite spectra it is first necessary to determine the time limits. This procedure is essential for numerical analysis considering that some of the ions ($E^* < E^*_{low}$) will never make any contribution to the flux at position Z.

An estimate for t_{min} is that time at which the most energetic ion in the spectrum has reached a position within 2σ of Z as shown in figure 9.

FIGURE 9

Distribution at t_{min} from Particle with E^*_{max}

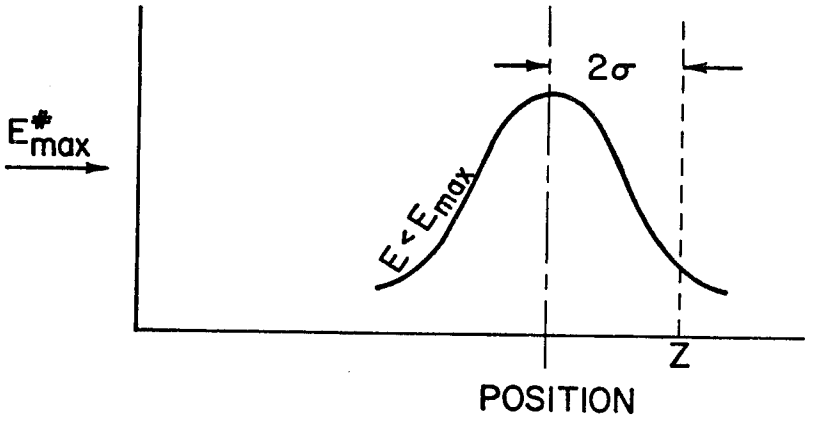

Thus t_{min} is the time when the mean location is

$$r_{min} = Z - 2\sigma\ (r_{min}, E^*_{max}) \tag{23}$$

Equation 23 requires an iterative evaluation but will converge within a few trials if an initial estimate of r is

$$r_{min} = Z - 2\sigma\ (R,\ E^*_{max}) \tag{24}$$

where R is the range when E^*_{max} has been reduced to 0.

The time, t_{min}, when an appreciable flux of particles will appear at position Z, is then given by equation 11 evaluated at the value of r determined in equation 23. Thus,

$$t_{min} = t\ (r, E^*)$$

$$\text{at } r = r_{min}$$

$$\text{when } E^* = E_{max}$$

The maximum time of interest, t_{max}, is given by the time when the lowest energy (E^*_{low}) particle can reach within 2σ of Z is approaching E = 0.

Hence, E^*_{low} is determined by the lowest energy (greater than E^*_{min}) which has range + 2σ which is greater than Z or:

$$R(E^*_{low}) + 2\sigma\ (R, E^*_{low}) \geq Z \tag{25}$$

At position Z, therefore, the limits on the flux are from t_{min} to t_{max} and the limits on the spectrumare E^*_{low} and E^*_{max}. It is possible at large values of Z that E^*_{low} will exceed E^*_{max} and no flux will occur. At small values of X, E^*_{low} may be less than E^*_{min} and all ions in the incident spectrum will give a contribution.

The flux at position Z can be evaluated by summing the contributions of each ion in the incident spectrum at a specific time, t, or:

$$F(t,Z) = \int_{\max(E^*_{min},E^*_{low})}^{E^*_{max}} Q(t,E^*)dE^* \qquad (26)$$

where $Q(t,E^*)$ is the flux at time t from that portion of the incident spectrum $S^*(E)dE^*$. $Q(t,E^*)$ may be evaluated by solving equation 17 at time t and V_* corresponding to E^* with the value of $C_o = S^*(E)dE^*$.

It is sometimes necessary to obtain a single energy to correlate with the flux at time t. This can be accomplished by determining the average energy as:

$$\bar{E}(t) = \frac{\int Q(t,E^*)\ E(E^*,Z)dE^*}{\int Q(t,E^*)dE^*} \qquad (27)$$

where $Q(t,E^*)$ is the same as in Equation 26, and

$E(E^*,Z)$ is the energy at position Z for an ion of incident energy E^* taken from equation 6.

The spectrum at position Z will be defined between the limits E_{min} and E_{max}, which are determined from the velocity calculated using equation 13 at times, t_{max} and t_{min}, and incident energies E^*_{min} and E^*_{max}, respectively.

The amplitude of the spectrum at the transmitted energy, E, is the summation of the contribution of all ions in the incident spectrum which have energy E at position Z. Hence

$$S(E,Z) = \int_{E^*} S^*(E^*)dE^*\ H(Z,E^*,E) \qquad (28)$$

where $S(E,Z)$ is the value of the spectrum at position Z

$S^*(E^*)dE^*$ is the incident spectrum.

$H(Z,E^*,E)$ is the portion of ions around E^* which have incident energy E at position Z, given by equation 20 with the value of C_o given by $S^*(E)dE^*$.

The relations developed above allow a complete, yet approximate, estimate of the flux and spectrum of an ion distribution as it passes through a material. It is readily applied to heavy ions or light ions of low energy as they pass through gases. It is however, applicable to solids and liquids as well.

These models have been incorporated into the T-DAMEN code so that any arbitrary incident spectrum can be modified by a protective gaseous layer of arbitrary pressure and temperature. The calculated form of the flux and spectra are identical in format to that in the case of no gases; consequently all subsequent response calculations (temperature displacement, etc.,) can be easily performed with the models discussed in Part II.[2]

An example of this model is given in figure 10. Energy spectra are shown for a mercury spectrum (Gaussian, 3 MeV ± 1 MeV) which is incident on a surface at a 6 meters location. Curves are shown for the case of no gas and 0.1, 0.2, 0.3 torr of neon, respectively.

At this point it should be noted that spectra, such as those in figure 7, calculated by these methods are approximations to the complex phenomena associated with ion transport in finite media. The previously presented comparison with a more complex solution for monoenergetic ions indicate that estimates of range and straggling of intermediate energy ion distribution differ by no more than 20%. This difference is (however) small in comparison to the large variation in range and straggling values associated with a broad spectrum of incident ions.

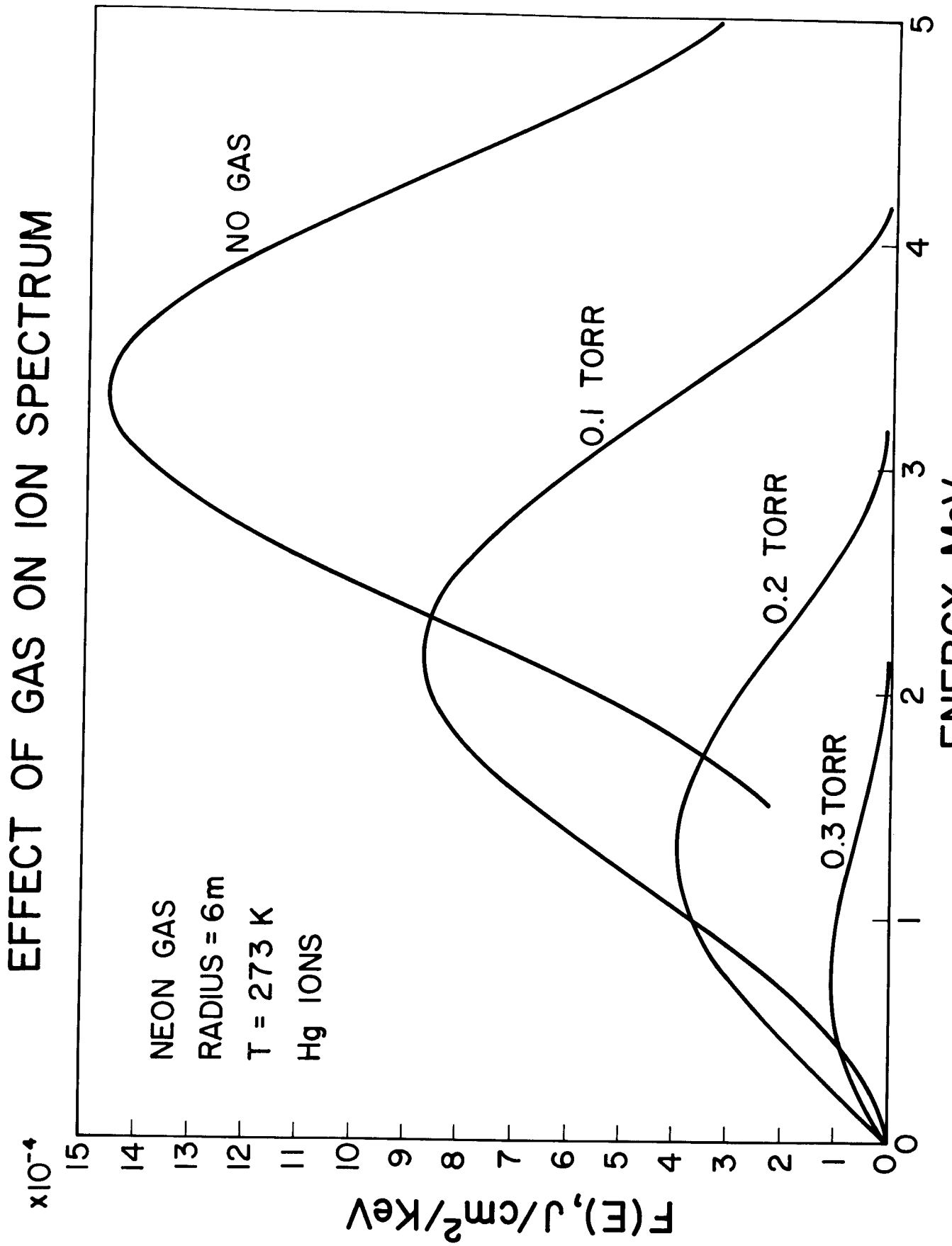
EFFECT OF GAS ON ION SPECTRUM
NEON GAS
RADIUS = 6m
T = 273 K
Hg IONS
NO GAS
0.1 TORR
0.2 TORR
0.3 TORR
F(E), J/cm²/KeV
x10⁻⁴
ENERGY, MeV
0
1
2
3
4
5
1
2
3
4
5
6
7
8
9
10
11
12
13
14
15

FIGURE 10

An additional caution should be noted when using data such as that in figure 7. The flux and associated spectra arriving at a point from a pulsed fusion source are functions of both the gas density and the path length. Hence, in contrast to modification of photon fluxes, results cannot be generalized to a normalized basis such as torr-meters of buffer gas.

III.B. Spectral Modification of Light Ions

If the energy of light ions is sufficiently high (> 10 keV/amu) a simple method can be developed to modify an incident spectrum by a gaseous layer. This procedure is based on the stopping power formulations and energy-location relations developed in Part II.[2] This formulation is considered accurate when the incident ion energy is high or when the range of the particle exceeds the thickness of the gas by a factor of 2 or more. In both cases the difference in path length and range is small and the standard deviation of the distribution of each ion is small compared to the distribution for a spectrum as a whole.

Part II gave relations which allowed the determination of the mean local energy of an ion of incident energy E*, as:

$$E = E(E^*,Z)$$

Here it is assumed that a relation can be developed which allows the determination of the mean time to reach position Z as:

$$t = t(E^*,Z)$$

Formulae for estimating these times are dependent on the stopping power regimes of the incident ion and will be developed later in this section.

If relations for energy and time as a function of position are known, the modified spectrum can be determined easily from:

$$S(E,Z) = S(E^*)dE^*/dE \tag{29}$$

where E is determined from the relation $E(E^*,Z)$,

dE is estimated from $E_N(E^*_N,Z) - E_{N-1}(E^*_{N-1},Z)$,

dE* is a specified discretization of the incident spectrum,

N is an arbitrary energy group in the spectrum.

The limits of the transmitted spectrum will be the energy of the maximum energy incident ion at position Z and the larger of a) the energy of the minimum energy incident ion at position Z, or b) the incident ion energy whose mean range is Z.

The flux can likewise be determined from the transformation

$$F(t) = S(E^*)dE^*/dt \tag{30}$$

where F is the flux at time t,

and dt is estimated from $t(E^*_{N-1},Z) - t(E^*_N,Z)$.

An outline of the processes described above is shown schematically in figure 11.

III.B.1. Time Functions

The mean time of an ion of incident energy E* to position Z can be estimated for light ions from stopping power relations discussed in Part II.[2] These relations were based upon a three region stopping power formulation. We will now develop formulae for the time associated with each energy interval. The summation of time for each interval then represents the total time to reach an energy E at position Z. We first of all note,

$$\frac{dE}{dx} = S_o(E/E_o)^{\frac{1}{2}} \tag{31}$$

Hence the mean time is

FIGURE 11

LIGHT ION ANALYSIS

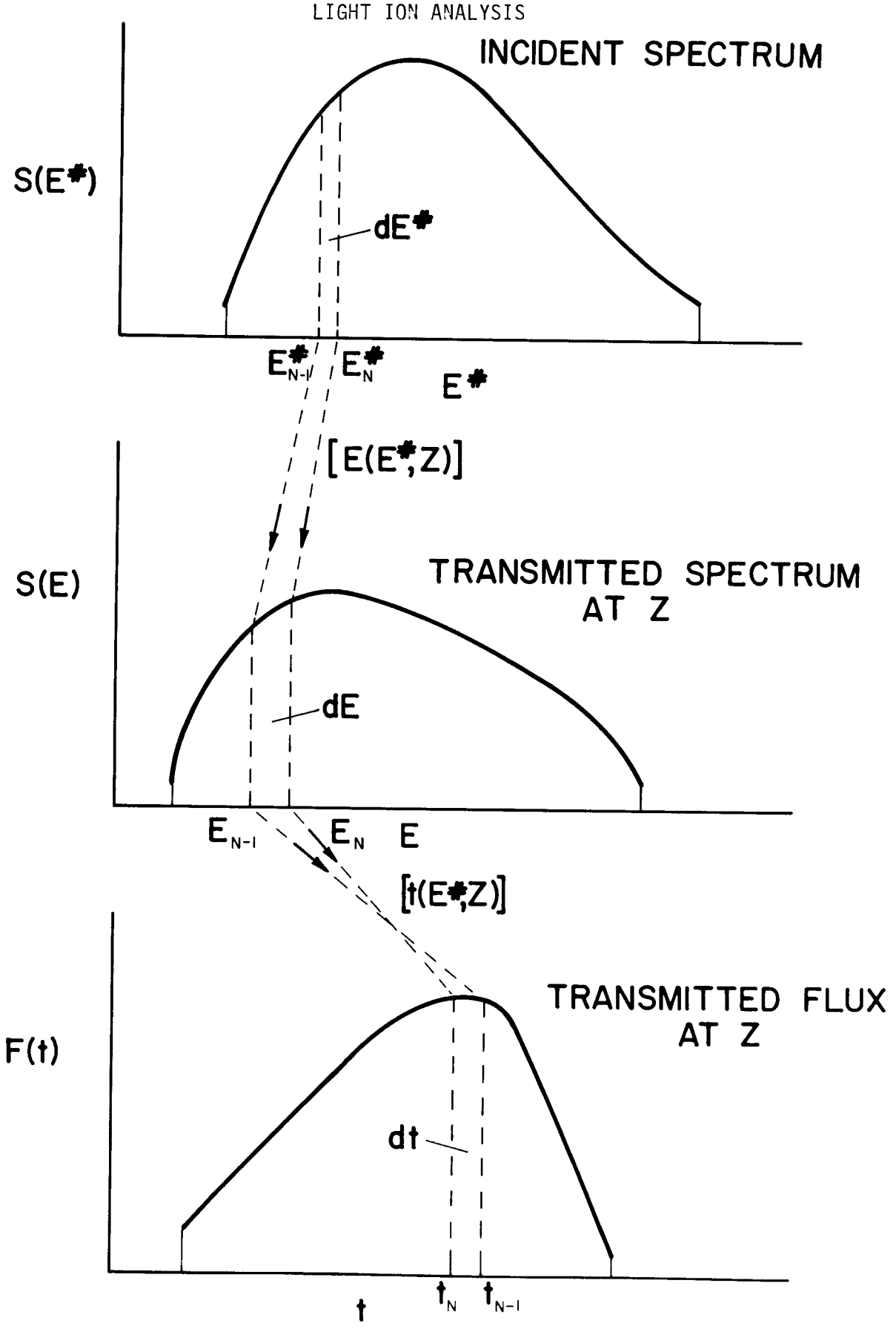

$$\langle t \rangle_1 = \int_E^{E^*} \frac{dE}{V\frac{dE}{dx}} \tag{32}$$

or

$$\langle t \rangle_1 = \int_E^{E^*} \frac{dE}{D\sqrt{E/M}\, S_o (E/E_o)^{\frac{1}{2}}} \tag{33}$$

which when integrated is

$$\langle t \rangle_1 = \frac{\sqrt{mE_o}}{DS_o} \ln E^*/E \tag{34}$$

where S_o = keV/cm

m = amu

E_o = keV

$D = 4.38 \times 10^7 \quad \frac{\text{cm amu}^{\frac{1}{2}}}{\text{sec kev}^{\frac{1}{2}}}$.

Equation 34 is valid until the local energy reaches about "2A" keV* in which case deceleration from nuclear processes must be considered. In this analysis it was assumed that the stopping power below 2A keV is a constant value equal to the value of equation 31 at 2A keV. Hence,

$$\frac{dE}{dx} = S_o \left(\frac{2A}{E_o}\right)^{\frac{1}{2}} \tag{35}$$

and defining the position at which that energy is reached as

$$Z_{2A} = \frac{2E_o^{\frac{1}{2}}}{S_o} (E_*^{\frac{1}{2}} - 2A^{\frac{1}{2}}) \tag{36}$$

the ion energy at any distance between Z_{2A} and 0 is determined by

*A here the atomic weight.

$$E(X) = 2A - S_o\ (2A/E_o)^{\frac{1}{2}}\ X \tag{37}$$

and the approximate time from Z_{2A} to position Z ($Z > Z_{2A}$) is

$$t' = \frac{Z - Z_{2A}}{[V(2A) + V\ (E(Z))]/2}$$

where V is the velocity corresponding to the energy at that point and E(Z) is taken from equation 37.

For the intermediate and high velocity regimes, regions 2 and 3, the relations for energy at any position were given in Part II[2] and are not repeated here. The most direct method for determining the time to an intermediate energy is to assume a piecewise linear velocity profile and defining 3 reference points.

X_1, V_1 - the velocity and position of the incident ion into either regions 2 or 3.

X_{mid}, V_{mid} - the velocity and position halfway between incidence and leaving regions 2 or 3.

X_2, V_2 - the velocity and position leaving regions 2 or 3.

A piecewise linear approximation between each point gives

$$t_{X_1 - X_{mid}} = \int_{X_1}^{X_{mid}} \frac{dx}{V}$$

$$t_{X_1 - X_{mid}} = B\ \ell n\ V_{mid}/V_1 \tag{38}$$

where

$$B = \frac{X_{mid} - X_1}{V_{mid} - V_1}$$

likewise

$$t_{X_{mid}-X_2} = B' \ \ell n \ V_2/V_{mid} \tag{39}$$

where

$$B' = \frac{X_2 - X_{mid}}{V_2 - V_{mid}}$$

the total transit time in any region is then

$$t_{X_1-X_2} = B \ \ell n \ V_{mid}/V_1 + B' \ \ell n \ V_2/V_{mid} \tag{40}$$

where the velocities are determined from the incident energy, $E(X_{mid})$, and $E(X_2)$ where X_2 is the position leaving the region or Z if X_2 is greater than Z.

The relations have all been incorporated into the T*DAMEN for modificatin of light ion spectra and, as in the case for heavy ions, have output formats which are compatible with the subsequent response calculations. An example of the modification of a tritium spectrum is shown in figure 12. In this case a 320 keV Maxwellian spectrum is shown at a position of 7 meters for a neon buffer gas at pressures of 0.1, 0.5, 1, and 2 torr, respectively.

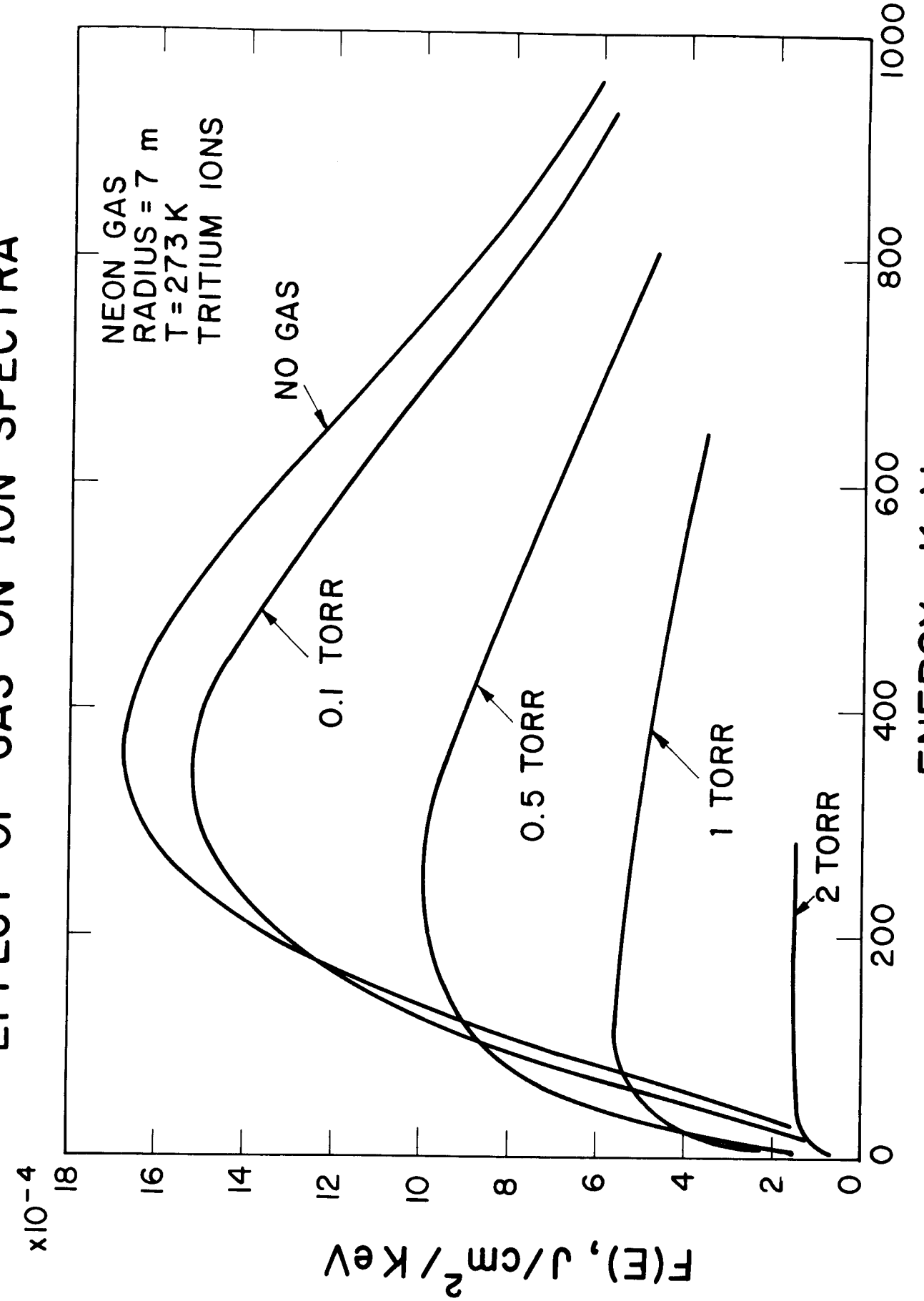
EFFECT OF GAS ON ION SPECTRA
NEON GAS
RADIUS = 7 m
T = 273 K
TRITIUM IONS
NO GAS
0.1 TORR
0.5 TORR
1 TORR
2 TORR
F(E), J/cm²/KeV
x10⁻⁴
ENERGY, KeV
0
2
4
6
8
10
12
14
16
18
0
200
400
600
800
1000

FIGURE 12

III.C. Energy Deposition in the Gas

If gaseous protection makes a significant modification of the ion spectra, a substantial amount of energy will be released in the gas. In the case of a pellet microexplosion, the spherical divergence of the flux makes the initial volumetric energy deposition very high even for modest gas pressures. This energy deposition is sufficient to heat and ionize the gas thereby setting up the condition for development of a shock wave and reradiation of the energy.

The methods discussed in the previous sections can be used to estimate the time dependent energy deposition at any point in the gaseous layer. For heavy ions the spectral dependence of the energy deposition can be developed starting from equation 4. If

$$R = C\, V_{\star}^{\frac{1}{1-k}}$$

then

$$\frac{dr}{dV} = \frac{C}{1-k}\, V^{\frac{k}{1-k}} \tag{41}$$

and using

$$\frac{dE}{dR} = \frac{dE}{dV}\,\frac{dV}{DR}$$

with

$$\frac{dE}{dV} = \frac{2mV}{(4.39\times10^{7})^{2}}$$

yields the energy deposition rate of

$$\frac{dE}{dr} = \frac{1-k}{C}\,\frac{m}{9.64\times10^{14}}\, V^{\frac{2k-1}{k-1}} \tag{42}$$

where V = instantaneous ion velocity, cm/sec

m = ion mass, amu

k,C are defined in equation 4

$\frac{dE}{dr}$ = energy deposition, keV/cm

These relations can be coupled with the relations for instantaneous flux and spectra (developed in section III.A) and with the appropriate divergence in spherical geometry to determine the deposition rate from an arbitrary ion spectra. The relations for the time, local energy, and energy deposition for light ions are readily applied to the appropriate flux and spectra in a spherical coordinate system to yield a similiar result.

These above relations are incorporated into the T*DAMEN code so that energy depositions can be obtained at arbitrary position in a buffer gas. This data can be used as the driving force for initiation of the general response of the gas including subsequent hydrodynamics and radiation.[14] Results of the energy deposition of Si and helium ions in 0.5 torr neon are shown in figure 13a and 13b. Spatial energy deposition profiles may be developed from these data by selecting a time along the abcissa and reading the cumulative deposition value at various positions. This self-consisent incorporation of the deposition in the gas into the T*DAMEN code allows assessment of the deposition in the gas and commensurate response of an exposed material for variations in gas type and density and ion spectra.

The data in figure 13 indicate that volumetric depositions of several hundred joules/cm^3 are released in less than 20 ns in the first few centimeters surrounding the thermonuclear source. These high depositions will cause ionization of the gas which in turn will allow energy to be radiated away upon recombination. In addition, the subsequent ion stopping will also be

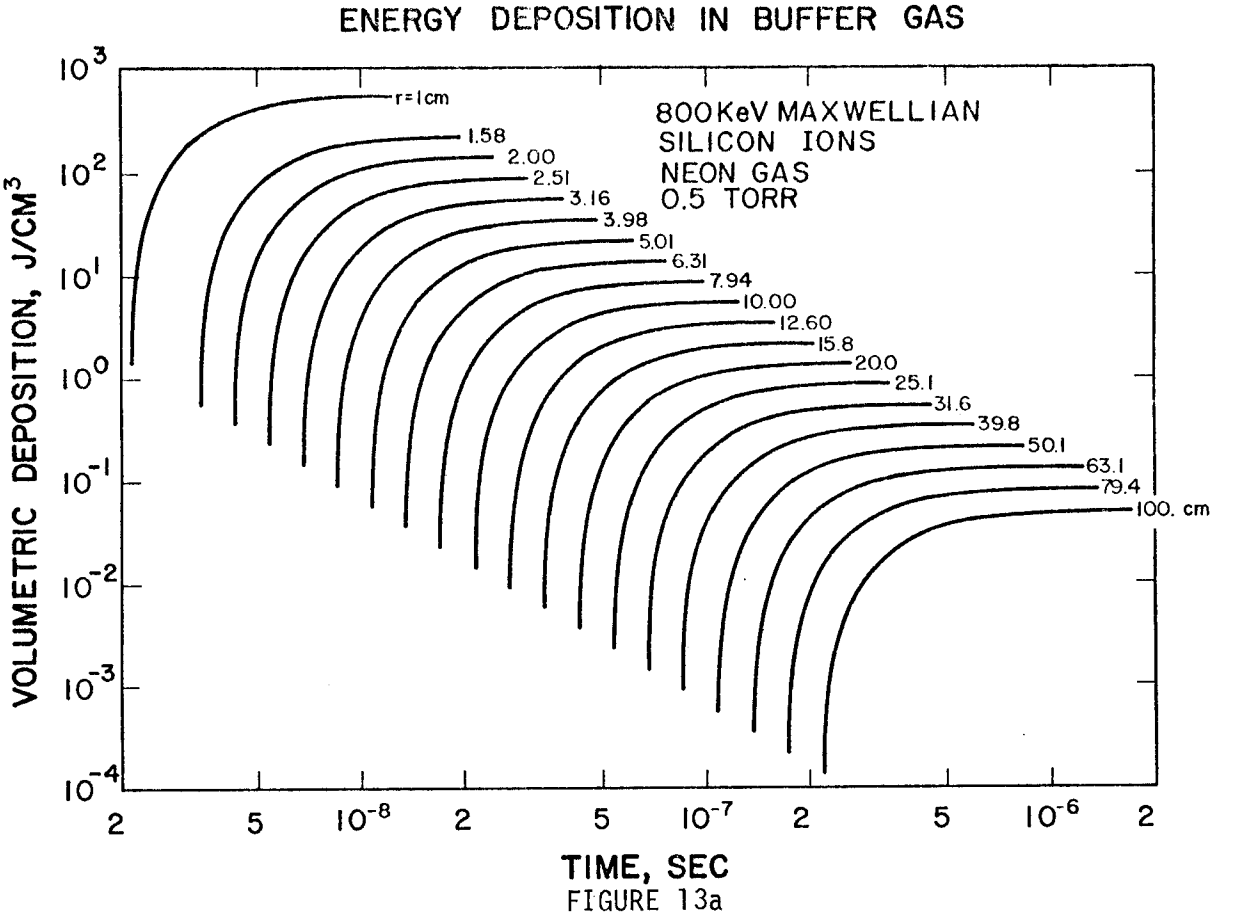

FIGURE 13a

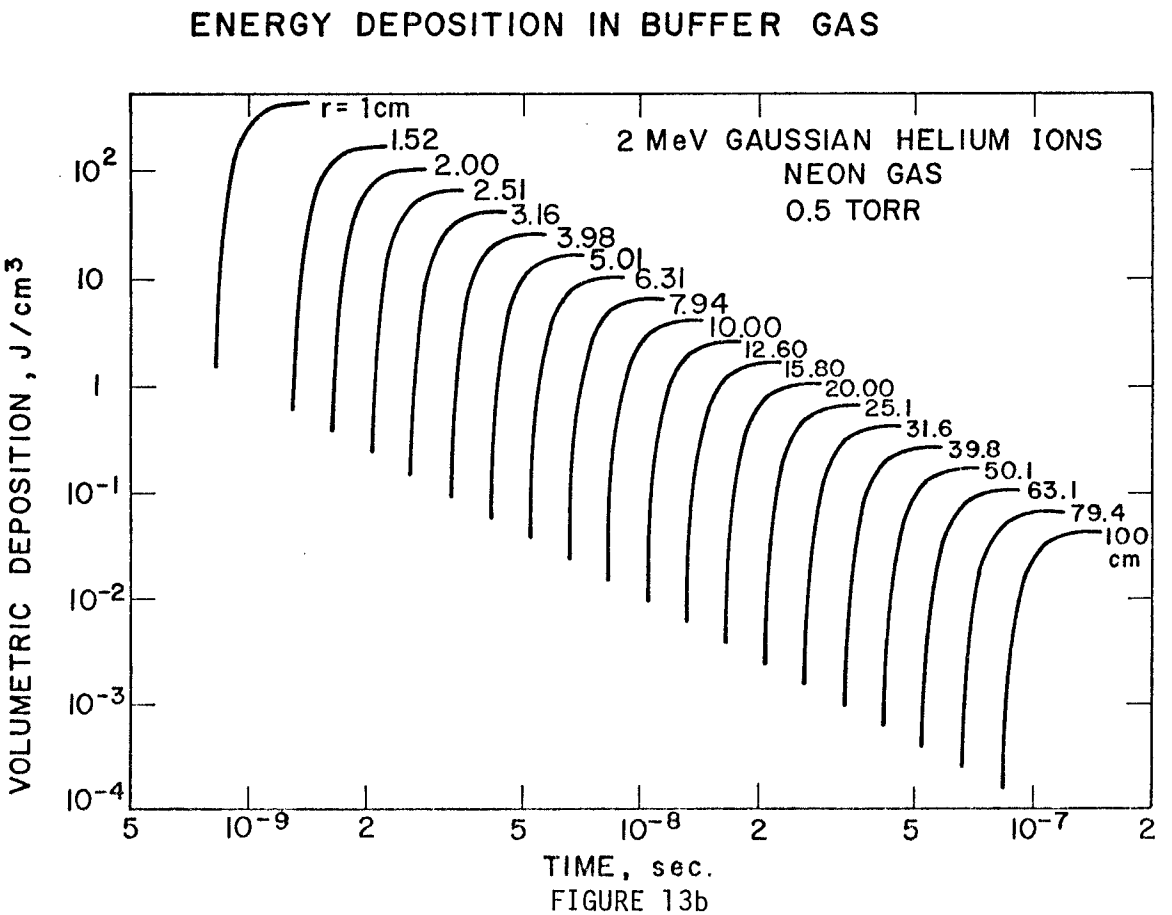

FIGURE 13b

influenced by this ionization, but the spectrum reaching the first wall will not be substantially different than predicted here since the first few centimeters make a small contribution to the spectra at radii of several meters.

It should also be noted that it is likely that the gas will reradiate the energy deposited by both ions and X-rays before it is exhausted from the chamber. This radiation must also be absorbed by the walls of the chamber. It is not the intent of this study to analyze this aspect of wall response although such analysis may be easily performed with a transient surface heat flux calculation which is a method also contained in the T-DAMEN code. The time scale for such energy release becomes the critical parameter in these calculations and estimates for the various radiation properties of gases are being assessed in reference 14.

IV. Modification of X-ray Spectra

Gaseous protection reduces the severity of the response of a material to a pulsed thermonuclear source not only because it stops or slows down energetic ions, but because it can significantly modify the X-ray spectrum as well. This modification is, however, extremely sensitive to the initial X-ray spectrum and the gas chosen. An example of this relationship is shown in figure 14 where the total cross section of He, Ne, and Xe are shown as a function of photon energy. These data are taken from the T*DAMEN code which are taken from the data of Biggs.[15]

The T*DAMEN code contains the ability to examine the X-ray deposition in as many as four successive layers. If the first layer is a gas, the spectra onto the second layer and the subsequent temperature response of the second layer give a measure of the protection provided by the gas against the initial radiation burst. An example of the modification of an initial 1 keV black body spectrum by 7 meters of 0.5 torr neon gas is shown in figure 15. It should be noted from these data that any single gas can appear transparent to radiation near an absorption edge and consequently mixtures of gases may be necessary. A more general study of the response of several materials to a variety of X-ray spectra and gases will be presented in the form of a parameter study in chapter V.

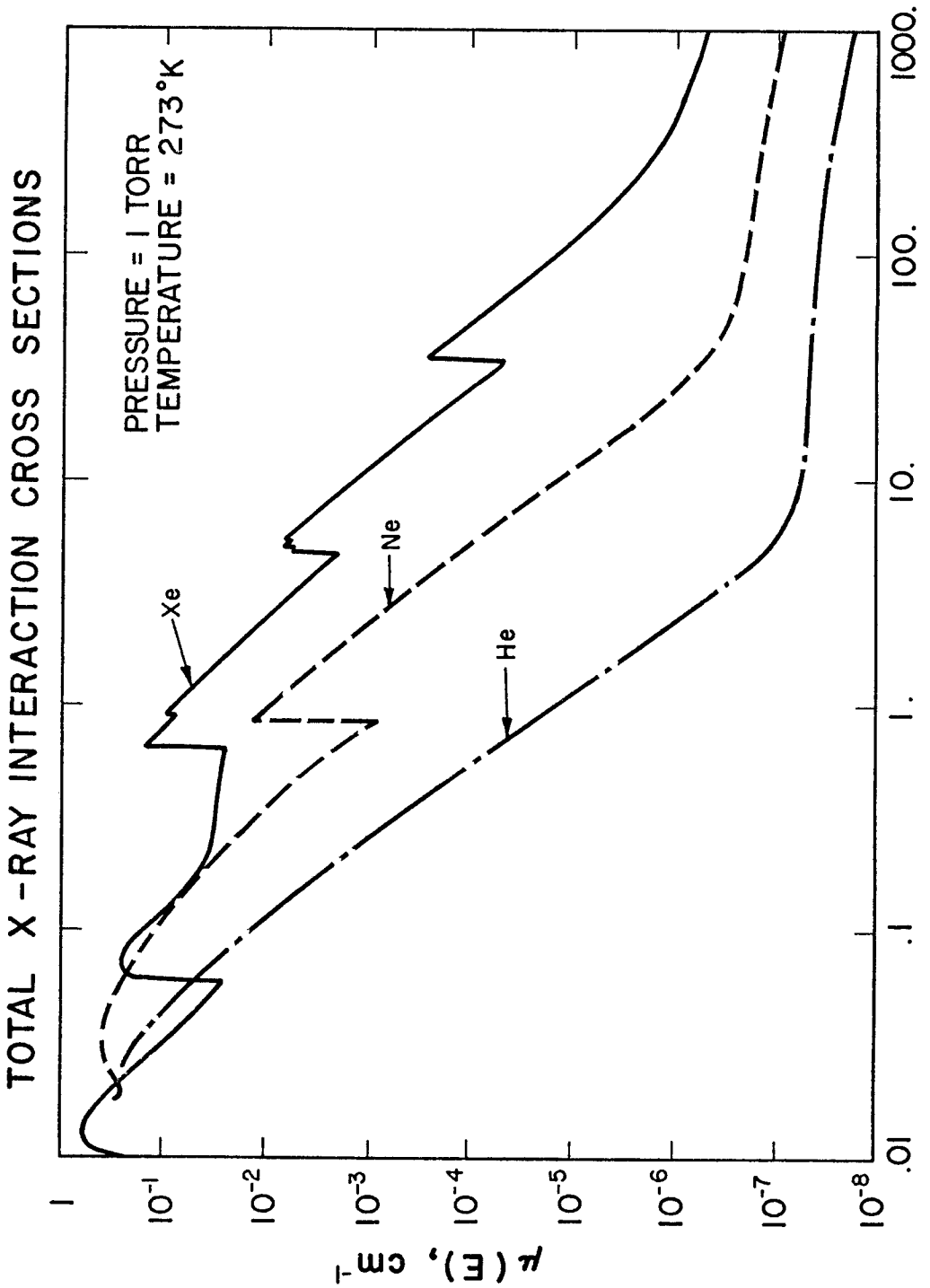
TOTAL X-RAY INTERACTION CROSS SECTIONS
PRESSURE = 1 TORR
TEMPERATURE = 273°K
Xe
Ne
He
μ (E), cm⁻¹
1
10⁻¹
10⁻²
10⁻³
10⁻⁴
10⁻⁵
10⁻⁶
10⁻⁷
10⁻⁸
.01
.1
1.
10.
100.
1000.
X-RAY ENERGY, KeV

FIGURE 14

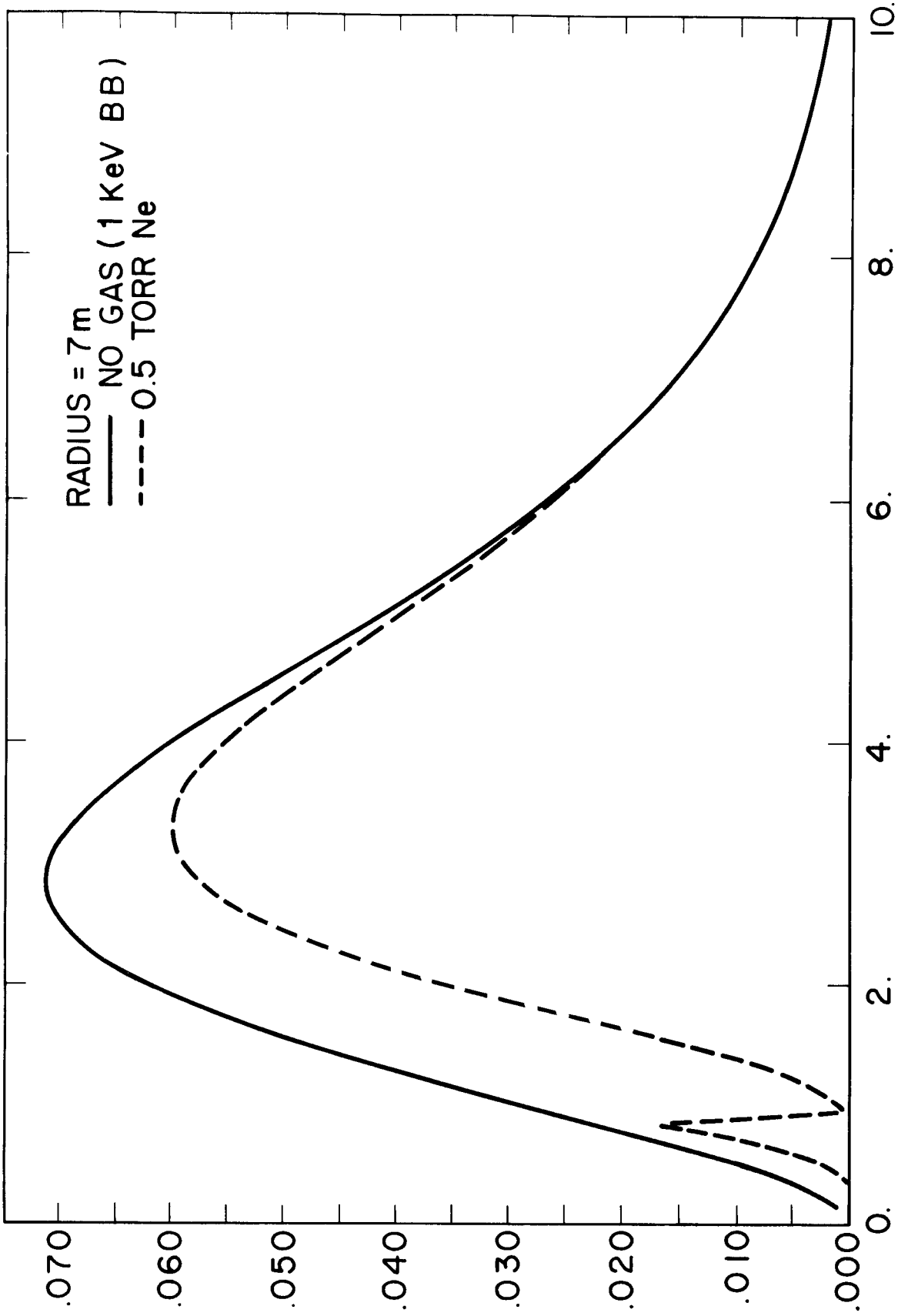
X-RAY SPECTRUM
RADIUS = 7m
NO GAS (1 KeV BB)
0.5 TORR Ne
F, JOULES/KEV/CM²
.000
.010
.020
.030
.040
.050
.060
.070
0.
2.
4.
6.
8.
10.
ENERGY, KEV

FIGURE 15

V. Application of Models to Photon and Ion Spectra

This chapter will give examples of the modification of the response of materials by introduction of various gases between the thermonuclear source and the exposed material. The first section contains a parameter study of the response to photon spectra while the second section contains a more general analysis of a complete spectra of ions and photons.

V.A. Parametric Analysis of Photon Response

The choice of materials and gaseous protection parameters in an inertial confinement reactor is extremely sensitive to the output characteristics of the microexplosion. As a consequence a study was performed here to examine the response of three materials to variations in X-ray spectra and X-ray radiation time. The results are presented in terms of general tables covering all parametric variations and selected curves demonstrating specific effects.

The parameters chosen in the analysis were:

Source

Spectrum - (Blackbody Temperature)

0.1 0.2 0.3 0.4 0.5 0.75 1 2 5 10

Duration (Seconds)

Impulse 10^{-11} 10^{-10} 10^{-9} 10^{-8} 10^{-7}

Gas

Type

He, Ne, Xe

Pressure (at 273°K) - Torr

0. 0.1 0.5 1 5 10

Material

C, Cu, Mo

All calculations were performed for temperature response at 2.82 meters from 1 MJ of X-ray output. This corresponds to a wall loading (in the absence of gas) of 1 J/cm^2. The areal density of gas protection is thus normalized to 2.82 times the gas pressure in torr-meters. The results are generalized in that the same response will be exhibited at a given areal density (torr-meters) for an equivalent bare wall loading. All results are to be interpreted as ΔT per J/cm^2 since the entire problem is linear with respect to flux. (Caution: the problem is, of course, not linear with respect to areal density of protective gas because of the exponential behavior of the absorption factors.)

Data are presented in tables V-1 to V-9. Each table represents the combination of one gas and material. Within each table are the variations of gas pressure, source time, and blackbody temperature.

Selected data from these tables are given in figures 16, 17, 18, and 19. The effect of gas type on the response of copper at 2.8 torr-meters is shown in figure 16 as a function of X-ray spectrum for a source duration of 1 nanosecond. The significant variation with the atomic number of the gas indicates that much greater pressures of the lighter gases will be required to achieve the same effect. Neon at 2.8 torr-meters reduces the temperature excursion by factors of 2-5 for blackbody spectra up to about 1 keV. Xenon essentially eliminates the X-ray temperature response for these spectra while helium gives only a small (10-30%) reduction for spectra at 0.1 to 0.3 keV. For blackbody spectra of 5 keV and above, all gases tend to lose their effectiveness as the cross sections become smaller.

Figure 17 shows the effect of various areal densities of gas for copper and neon as a function of source temperature at a 1 nanosecond source duration. These data demonstrate the exponential behavior of response on the torr-meters

of gas present. The irregularities in the curves at higher gas densities are due to the combination of absorption edges in the gas and those of the matter in which the temperature is calculated. A maxima develops in the curves as gas density is increased because the gas tends to preferentially absorb lower energy X-rays. The higher energy X-rays are allowed to pass into the copper and can still result in a significant temperature response.

The effect of source duration is shown in figure 18 for copper and neon at 2.8 torr-meters. A substantial reduction from the adiabatic response is noted due to the conductivity of the material. The effect is most significant for lower source temperatures where gradients near the surface are the highest and the maximum reduction due to longer source times is observed in copper due to its high thermal diffusivity. These data are compatible with the estimates made in Part I[1] which predicted the time scales for which the adiabatic assumption was valid.

Figure 19 shows variation in the material on response with neon at 2.8 torr-meters and a source duration of 1 nanosecond. These data show the difference in both X-ray absorption properties and thermal properties of the material. In general the temperature response is shown to be greater with materials of higher atomic number. This effect is especially evident for higher energy spectra in which carbon (Z=6) shows a marked lower response than either copper or molybdenum.

Table V.1. Normalized Thermal Response from X-Rays in Carbon with Helium Gas Protection

Surface Temperature Rise
[°C per J/cm^2]
(Gas at 273 °K)

log Δt (sec)	BLACKBODY TEMPERATURE (KEV) .1	.2	.3	.4	.5	.75	1.	2.	5.	10.
	TORR=0.									
ADB	.838+4	.456+4	.230+4	.144+4	.890+3	.378+3	.198+3	.407+2	.312+1	.459+0
-11	.795+4	.440+4	.224+4	.140+4	.873+3	.372+3	.195+3	.400+2	.311+1	.459+0
-10	.723+4	.411+4	.213+4	.134+4	.840+3	.361+3	.190+3	.388+2	.310+1	.459+0
-9	.574+4	.344+4	.187+4	.118+4	.759+3	.332+3	.177+3	.360+2	.306+1	.458+0
-8	.363+4	.239+4	.140+4	.915+3	.610+3	.278+3	.152+3	.314+2	.294+1	.455+0
-7	.178+4	.133+4	.872+3	.600+3	.423+3	.207+3	.117+3	.257+2	.268+1	.447+0
	TORR=.1									
ADB	.757+4	.439+4	.225+4	.142+4	.881+3	.376+3	.197+3	.405+2	.312+1	.459+0
-11	.722+4	.425+4	.220+4	.138+4	.864+3	.370+3	.194+3	.399+2	.311+1	.459+0
-10	.661+4	.398+4	.209+4	.132+4	.832+3	.359+3	.189+3	.386+2	.310+1	.459+0
-9	.532+4	.336+4	.184+4	.117+4	.753+3	.331+3	.176+3	.359+2	.305+1	.458+0
-8	.340+4	.234+4	.139+4	.907+3	.606+3	.277+3	.151+3	.313+2	.294+1	.455+0
-7	.168+4	.131+4	.864+3	.597+3	.421+3	.206+3	.117+3	.257+2	.268+1	.447+0
	TORR=.5									
ADB	.674+4	.417+4	.217+4	.137+4	.860+3	.369+3	.194+3	.399+2	.312+1	.459+0
-11	.643+4	.404+4	.212+4	.134+4	.844+3	.364+3	.192+3	.393+2	.311+1	.459+0
-10	.589+4	.379+4	.202+4	.128+4	.814+3	.353+3	.187+3	.381+2	.309+1	.459+0
-9	.474+4	.320+4	.178+4	.114+4	.737+3	.326+3	.174+3	.355+2	.305+1	.458+0
-8	.303+4	.225+4	.135+4	.887+3	.596+3	.274+3	.150+3	.311+2	.293+1	.455+0
-7	.150+4	.126+4	.845+3	.587+3	.415+3	.204+3	.116+3	.256+2	.268+1	.447+0
	TORR=1.									
ADB	.624+4	.398+4	.211+4	.134+4	.840+3	.362+3	.191+3	.392+2	.311+1	.459+0
-11	.594+4	.386+4	.206+4	.131+4	.825+3	.357+3	.189+3	.386+2	.310+1	.459+0
-10	.544+4	.362+4	.196+4	.125+4	.796+3	.347+3	.184+3	.376+2	.309+1	.459+0
-9	.437+4	.307+4	.173+4	.111+4	.723+3	.321+3	.172+3	.351+2	.305+1	.458+0
-8	.279+4	.216+4	.132+4	.869+3	.586+3	.270+3	.148+3	.308+2	.293+1	.455+0
-7	.137+4	.121+4	.828+3	.578+3	.410+3	.203+3	.115+3	.255+2	.267+1	.447+0
	TORR=5.									
ADB	.418+4	.302+4	.174+4	.112+4	.731+3	.325+3	.174+3	.351+2	.306+1	.459+0
-11	.397+4	.294+4	.171+4	.110+4	.720+3	.320+3	.172+3	.347+2	.307+1	.458+0
-10	.364+4	.278+4	.164+4	.106+4	.698+3	.313+3	.168+3	.341+2	.305+1	.458+0
-9	.294+4	.240+4	.147+4	.957+3	.642+3	.292+3	.159+3	.324+2	.301+1	.457+0
-8	.189+4	.175+4	.114+4	.770+3	.532+3	.251+3	.139+3	.292+2	.290+1	.454+0
-7	.924+3	.101+4	.739+3	.528+3	.382+3	.192+3	.111+3	.247+2	.265+1	.446+0
	TORR=10.									
ADB	.285+4	.232+4	.145+4	.947+3	.639+3	.292+3	.159+3	.322+2	.303+1	.458+0
-11	.270+4	.227+4	.142+4	.932+3	.631+3	.289+3	.157+3	.319+2	.302+1	.458+0
-10	.248+4	.217+4	.137+4	.904+3	.614+3	.283+3	.154+3	.315+2	.301+1	.457+0
-9	.203+4	.191+4	.125+4	.832+3	.572+3	.267+3	.147+3	.303+2	.297+1	.457+0
-8	.134+4	.143+4	.998+3	.687+3	.484+3	.234+3	.131+3	.279+2	.289+1	.454+0
-7	.672+3	.864+3	.665+3	.485+3	.357+3	.183+3	.106+3	.240+2	.262+1	.446+0

Table V.2. Normalized Thermal Response from X-Rays in Carbon with Neon Gas Protection

Surface Temperature Rise
[°C per J/cm^2]
(Gas at 273 °K)

log Δt (sec)	BLACKBODY TEMPERATURE (KEV) .1	.2	.3	.4	.5	.75	1.	2.	5.	10.
	TORR=0.									
ADB	.838+4	.456+4	.230+4	.144+4	.890+3	.378+3	.198+3	.407+2	.312+1	.459+0
-11	.795+4	.440+4	.224+4	.140+4	.873+3	.372+3	.195+3	.400+2	.311+1	.459+0
-10	.723+4	.411+4	.213+4	.134+4	.840+3	.361+3	.190+3	.388+2	.310+1	.459+0
-9	.574+4	.344+4	.187+4	.118+4	.759+3	.332+3	.177+3	.360+2	.306+1	.458+0
-8	.363+4	.239+4	.140+4	.915+3	.610+3	.278+3	.152+3	.314+2	.294+1	.455+0
-7	.178+4	.133+4	.872+3	.600+3	.423+3	.207+3	.117+3	.257+2	.266+1	.447+0
	TORR=.1									
ADB	.524+4	.349+4	.186+4	.118+4	.750+3	.326+3	.173+3	.350+2	.299+1	.447+0
-11	.501+4	.338+4	.182+4	.115+4	.737+3	.321+3	.170+3	.345+2	.298+1	.447+0
-10	.461+4	.318+4	.174+4	.111+4	.711+3	.312+3	.166+3	.336+2	.297+1	.447+0
-9	.373+4	.270+4	.154+4	.986+3	.647+3	.289+3	.156+3	.315+2	.292+1	.446+0
-8	.239+4	.191+4	.117+4	.773+3	.525+3	.244+3	.134+3	.279+2	.281+1	.443+0
-7	.117+4	.108+4	.733+3	.513+3	.367+3	.183+3	.105+3	.233+2	.257+1	.436+0
	TORR=.5									
ADB	.211+4	.175+4	.104+4	.666+3	.451+3	.205+3	.113+3	.228+2	.256+1	.408+0
-11	.202+4	.171+4	.102+4	.655+3	.445+3	.203+3	.112+3	.226+2	.256+1	.408+0
-10	.187+4	.163+4	.980+3	.634+3	.432+3	.199+3	.110+3	.223+2	.255+1	.408+0
-9	.155+4	.144+4	.884+3	.579+3	.400+3	.187+3	.104+3	.214+2	.251+1	.407+0
-8	.104+4	.107+4	.694+3	.469+3	.333+3	.162+3	.923+2	.197+2	.242+1	.405+0
-7	.527+3	.629+3	.444+3	.319+3	.238+3	.124+3	.741+2	.172+2	.223+1	.400+0
	TORR=1.									
ADB	.938+3	.954+3	.604+3	.400+3	.282+3	.135+3	.769+2	.165+2	.220+1	.373+0
-11	.890+3	.937+3	.595+3	.394+3	.279+3	.133+3	.764+2	.164+2	.220+1	.373+0
-10	.828+3	.904+3	.578+3	.384+3	.273+3	.131+3	.753+2	.162+2	.219+1	.373+0
-9	.707+3	.818+3	.531+3	.357+3	.256+3	.125+3	.722+2	.158+2	.216+1	.373+0
-8	.502+3	.638+3	.430+3	.297+3	.218+3	.110+3	.653+2	.149+2	.209+1	.371+0
-7	.271+3	.391+3	.281+3	.206+3	.159+3	.867+2	.537+2	.134+2	.194+1	.368+0
	TORR=5.									
ADB	.102+3	.904+2	.656+2	.494+2	.410+2	.248+2	.176+2	.596+1	.119+1	.262+0
-11	.749+2	.896+2	.651+2	.490+2	.408+2	.247+2	.175+2	.595+1	.119+1	.262+0
-10	.553+2	.881+2	.640+2	.483+2	.403+2	.245+2	.174+2	.595+1	.119+1	.262+0
-9	.411+2	.836+2	.610+2	.463+2	.388+2	.239+2	.171+2	.592+1	.118+1	.262+0
-8	.307+2	.720+2	.530+2	.409+2	.350+2	.224+2	.163+2	.584+1	.117+1	.262+0
-7	.196+2	.499+2	.376+2	.304+2	.273+2	.192+2	.147+2	.569+1	.114+1	.261+0
	TORR=10.									
ADB	.699+2	.153+2	.113+2	.958+1	.950+1	.781+1	.698+1	.367+1	.871+1	.248+0
-11	.432+2	.152+2	.112+2	.953+1	.946+1	.779+1	.697+1	.367+1	.871+0	.248+0
-10	.243+2	.150+2	.110+2	.941+1	.937+1	.775+1	.695+1	.367+1	.871+1	.247+0
-9	.120+2	.144+2	.106+2	.909+1	.912+1	.764+1	.690+1	.366+1	.870+0	.247+0
-8	.639+1	.127+2	.939+1	.821+1	.841+1	.734+1	.674+1	.365+1	.867+0	.247+0
-7	.355+1	.914+1	.687+1	.636+1	.689+1	.669+1	.641+1	.363+1	.861+0	.247+0

Table V.3. Normalized Thermal Response from X-Rays in Carbon with Xenon Gas Protection

Surface Temperature Rise
[°C per J/cm^2]
(Gas at 273 °K)

log Δt (sec)	BLACKBODY TEMPERATURE (KEV) .1	.2	.3	.4	.5	.75	1.	2.	5.	10.
	TORR=0.									
ADB	.838+4	.456+4	.230+4	.144+4	.890+3	.378+3	.198+3	.407+2	.312+1	.459+0
-11	.795+4	.440+4	.224+4	.140+4	.873+3	.372+3	.195+3	.400+2	.311+1	.459+0
-10	.723+4	.411+4	.213+4	.134+4	.840+3	.361+3	.190+3	.388+2	.310+1	.459+0
-9	.574+4	.344+4	.187+4	.118+4	.759+3	.332+3	.177+3	.360+2	.306+1	.458+0
-8	.363+4	.239+4	.140+4	.915+3	.610+3	.278+3	.152+3	.314+2	.294+1	.455+0
-7	.178+4	.133+4	.872+3	.600+3	.423+3	.207+3	.117+3	.257+2	.268+1	.447+0
	TORR=.1									
ADB	.304+4	.171+4	.820+3	.502+3	.314+3	.137+3	.777+2	.178+2	.166+1	.364+0
-11	.291+4	.165+4	.797+3	.488+3	.307+3	.134+3	.767+2	.175+2	.168+1	.364+0
-10	.266+4	.153+4	.752+3	.461+3	.294+3	.130+3	.746+2	.170+2	.166+1	.363+0
-9	.213+4	.127+4	.645+3	.398+3	.261+3	.119+3	.693+2	.160+2	.167+1	.363+0
-8	.134+4	.843+3	.462+3	.293+3	.203+3	.982+2	.596+2	.143+2	.166+1	.362+0
-7	.650+3	.435+3	.266+3	.181+3	.137+3	.744+2	.478+2	.126+2	.162+1	.358+0
	TORR=.5									
ADB	.112+3	.694+2	.355+2	.240+2	.189+2	.137+2	.111+2	.456+1	.859+0	.240+0
-11	.108+3	.671+2	.346+2	.235+2	.186+2	.136+2	.111+2	.455+1	.859+0	.240+0
-10	.994+2	.627+2	.328+2	.224+2	.180+2	.135+2	.110+2	.453+1	.859+0	.240+0
-9	.802+2	.524+2	.284+2	.198+2	.167+2	.130+2	.108+2	.449+1	.858+0	.240+0
-8	.510+2	.353+2	.206+2	.154+2	.141+2	.121+2	.103+2	.442+1	.857+0	.240+0
-7	.245+2	.180+2	.120+2	.106+2	.111+2	.110+2	.971+1	.433+1	.853+0	.239+0
	TORR=1.									
ADB	.205+1	.144+1	.106+1	.153+1	.232+1	.361+1	.378+1	.215+1	.551+0	.188+0
-11	.198+1	.140+1	.105+1	.152+1	.232+1	.360+1	.378+1	.215+1	.551+0	.188+0
-10	.184+1	.132+1	.101+1	.150+1	.231+1	.360+1	.377+1	.215+1	.551+0	.188+0
-9	.151+1	.113+1	.922+0	.144+1	.227+1	.358+1	.377+1	.215+1	.551+0	.188+0
-8	.990+0	.792+0	.754+0	.135+1	.221+1	.356+1	.375+1	.215+1	.550+0	.188+0
-7	.487+0	.420+0	.551+0	.122+1	.212+1	.350+1	.371+1	.213+1	.549+0	.188+0
	TORR=5.									
ADB	.285-12	.946-11	.217-4	.242-2	.173-1	.539-1	.758-1	.108+0	.132+0	.986-1
-11	.281-12	.945-11	.217-4	.242-2	.173-1	.539-1	.758-1	.108+0	.132+0	.986-1
-10	.273-12	.943-11	.217-4	.242-2	.173-1	.539-1	.757-1	.108+0	.132+0	.986-1
-9	.251-12	.937-11	.216-4	.242-2	.173-1	.539-1	.757-1	.108+0	.132+0	.986-1
-8	.198-12	.920-11	.216-4	.242-2	.173-1	.538-1	.756-1	.108+0	.132+0	.986-1
-7	.118-12	.880-11	.213-4	.240-2	.172-1	.536-1	.754-1	.107+0	.132+0	.986-1
	TORR=10.									
ADB	.274-27	.186-21	.114-8	.123-4	.452-3	.156-2	.246-2	.185-1	.712-1	.736-1
-11	.271-27	.186-21	.113-8	.123-4	.452-3	.156-2	.246-2	.185-1	.712-1	.736-1
-10	.264-27	.185-21	.113-8	.123-4	.452-3	.156-2	.246-2	.185-1	.712-1	.736-1
-9	.246-27	.185-21	.113-8	.123-4	.452-3	.155-2	.246-2	.185-1	.712-1	.736-1
-8	.201-27	.183-21	.113-8	.123-4	.451-3	.155-2	.246-2	.185-1	.712-1	.736-1
-7	.125-27	.177-21	.112-8	.122-4	.450-3	.155-2	.245-2	.185-1	.712-1	.736-1

Table V.4. Normalized Thermal Response from X-Rays in Copper with Helium Gas Protection

Surface Temperature Rise
[°C per J/cm^2]
(Gas at 273 °K)

log Δt (sec)	BLACKBODY TEMPERATURE (KEV) .1	.2	.3	.4	.5	.75	1.	2.	5.	10.
	TORR=0.									
ADB	.248+5	.139+5	.116+5	.905+4	.741+4	.426+4	.285+4	.800+3	.193+3	.553+2
-11	.183+5	.115+5	.997+4	.798+4	.660+4	.389+4	.261+4	.764+3	.190+3	.549+2
-10	.122+5	.868+4	.778+4	.644+4	.541+4	.332+4	.225+4	.705+3	.185+3	.541+2
-9	.616+4	.507+4	.474+4	.413+4	.357+4	.236+4	.165+4	.593+3	.173+3	.523+2
-8	.247+4	.226+4	.219+4	.202+4	.183+4	.135+4	.100+4	.443+3	.154+3	.488+2
-7	.859+3	.832+3	.821+3	.790+3	.749+3	.622+3	.507+3	.291+3	.125+3	.427+2
	TORR=.1									
ADB	.216+5	.133+5	.114+5	.897+4	.736+4	.425+4	.285+4	.799+3	.193+3	.553+2
-11	.165+5	.112+5	.985+4	.793+4	.657+4	.388+4	.261+4	.764+3	.190+3	.549+2
-10	.112+5	.849+4	.772+4	.641+4	.540+4	.332+4	.225+4	.705+3	.185+3	.541+2
-9	.577+4	.499+4	.471+4	.411+4	.357+4	.236+4	.165+4	.593+3	.173+3	.523+2
-8	.233+4	.223+4	.218+4	.201+4	.182+4	.134+4	.100+4	.443+3	.154+3	.488+2
-7	.815+3	.823+3	.818+3	.789+3	.748+3	.621+3	.507+3	.291+3	.125+3	.427+2
	TORR=.5									
ADB	.169+5	.123+5	.110+5	.880+4	.727+4	.422+4	.283+4	.798+3	.193+3	.553+2
-11	.134+5	.105+5	.959+4	.781+4	.650+4	.386+4	.260+4	.763+3	.190+3	.549+2
-10	.940+4	.807+4	.756+4	.633+4	.535+4	.330+4	.224+4	.705+3	.185+3	.541+2
-9	.500+4	.479+4	.463+4	.407+4	.355+4	.235+4	.165+4	.593+3	.173+3	.523+2
-8	.206+4	.216+4	.215+4	.200+4	.181+4	.134+4	.100+4	.443+3	.154+3	.488+2
-7	.724+3	.799+3	.808+3	.784+3	.745+3	.620+3	.506+3	.290+3	.125+3	.427+2
	TORR=1.									
ADB	.141+5	.116+5	.107+5	.866+4	.719+4	.419+4	.282+4	.797+3	.193+3	.553+2
-11	.114+5	.996+4	.938+4	.770+4	.645+4	.384+4	.259+4	.762+3	.190+3	.549+2
-10	.816+4	.772+4	.742+4	.626+4	.531+4	.329+4	.223+4	.704+3	.185+3	.541+2
-9	.444+4	.463+4	.457+4	.404+4	.353+4	.235+4	.164+4	.592+3	.173+3	.523+2
-8	.185+4	.210+4	.212+4	.198+4	.181+4	.134+4	.100+4	.443+3	.154+3	.488+2
-7	.655+3	.777+3	.799+3	.779+3	.743+3	.619+3	.506+3	.290+3	.125+3	.427+2
	TORR=5.									
ADB	.695+4	.925+4	.973+4	.814+4	.688+4	.408+4	.277+4	.790+3	.193+3	.553+2
-11	.588+4	.810+4	.856+4	.728+4	.619+4	.375+4	.254+4	.756+3	.190+3	.548+2
-10	.451+4	.641+4	.683+4	.595+4	.512+4	.322+4	.220+4	.699+3	.184+3	.541+2
-9	.266+4	.394+4	.425+4	.387+4	.342+4	.231+4	.162+4	.589+3	.173+3	.522+2
-8	.117+4	.182+4	.199+4	.191+4	.176+4	.132+4	.991+3	.442+3	.154+3	.488+2
-7	.425+3	.679+3	.751+3	.752+3	.726+3	.613+3	.503+3	.290+3	.125+3	.427+2
	TORR=10.									
ADB	.440+4	.804+4	.912+4	.780+4	.667+4	.400+4	.272+4	.784+3	.193+3	.552+2
-11	.378+4	.707+4	.803+4	.698+4	.600+4	.368+4	.251+4	.751+3	.190+3	.548+2
-10	.299+4	.564+4	.642+4	.572+4	.498+4	.316+4	.217+4	.695+3	.184+3	.540+2
-9	.184+4	.349+4	.401+4	.373+4	.333+4	.227+4	.161+4	.587+3	.173+3	.522+2
-8	.839+3	.163+4	.188+4	.185+4	.172+4	.131+4	.983+3	.440+3	.154+3	.488+2
-7	.309+3	.610+3	.713+3	.730+3	.712+3	.607+3	.499+3	.289+3	.125+3	.427+2

Table V.5. Normalized Thermal Response from X-Rays in Copper with Neon Gas Protection

Surface Temperature Rise
[°C per J/cm^2]
(Gas at 273 °K)

log Δt (sec)	BLACKBODY TEMPERATURE (KEV)									
	.1	.2	.3	.4	.5	.75	1.	2.	5.	10.
	TORR=0.									
ADB	.248+5	.139+5	.116+5	.905+4	.741+4	.426+4	.285+4	.800+3	.193+3	.553+2
-11	.183+5	.115+5	.997+4	.798+4	.660+4	.389+4	.261+4	.764+3	.190+3	.549+2
-10	.122+5	.868+4	.778+4	.644+4	.541+4	.332+4	.225+4	.705+3	.185+3	.541+2
-9	.616+4	.507+4	.474+4	.413+4	.357+4	.236+4	.165+4	.593+3	.173+3	.523+2
-8	.247+4	.226+4	.219+4	.202+4	.183+4	.135+4	.100+4	.443+3	.154+3	.488+2
-7	.859+3	.832+3	.821+3	.790+3	.749+3	.622+3	.507+3	.291+3	.125+3	.427+2
	TORR=.1									
ADB	.113+5	.974+4	.911+4	.751+4	.631+4	.378+4	.255+4	.756+3	.190+3	.549+2
-11	.921+4	.843+4	.800+4	.671+4	.568+4	.348+4	.236+4	.725+3	.187+3	.545+2
-10	.671+4	.659+4	.638+4	.549+4	.472+4	.299+4	.205+4	.673+3	.182+3	.538+2
-9	.371+4	.401+4	.397+4	.358+4	.317+4	.217+4	.153+4	.571+3	.171+3	.520+2
-8	.157+4	.184+4	.187+4	.178+4	.165+4	.125+4	.947+3	.432+3	.153+3	.487+2
-7	.558+3	.682+3	.706+3	.703+3	.683+3	.586+3	.485+3	.286+3	.125+3	.426+2
	TORR=.5									
ADB	.329+4	.453+4	.475+4	.435+4	.387+4	.259+4	.181+4	.633+3	.180+3	.537+2
-11	.288+4	.405+4	.428+4	.396+4	.356+4	.243+4	.171+4	.613+3	.178+3	.534+2
-10	.230+4	.333+4	.353+4	.334+4	.305+4	.215+4	.153+4	.578+3	.175+3	.528+2
-9	.143+4	.216+4	.232+4	.229+4	.215+4	.163+4	.120+4	.507+3	.166+3	.513+2
-8	.657+3	.104+4	.114+4	.119+4	.118+4	.990+3	.787+3	.397+3	.150+3	.483+2
-7	.243+3	.398+3	.443+3	.485+3	.508+3	.483+3	.421+3	.270+3	.123+3	.424+2
	TORR=1.									
ADB	.144+4	.235+4	.259+4	.258+4	.244+4	.182+4	.134+4	.542+3	.172+3	.526+2
-11	.128+4	.215+4	.238+4	.239+4	.228+4	.173+4	.128+4	.529+3	.171+3	.523+2
-10	.107+4	.183+4	.202+4	.207+4	.200+4	.156+4	.117+4	.506+3	.168+3	.518+2
-9	.705+3	.125+4	.140+4	.149+4	.149+4	.123+4	.963+3	.454+3	.161+3	.506+2
-8	.343+3	.633+3	.722+3	.810+3	.856+3	.790+3	.661+3	.368+3	.147+3	.478+2
-7	.130+3	.247+3	.287+3	.341+3	.382+3	.401+3	.368+3	.257+3	.122+3	.422+2
	TORR=5.									
ADB	.124+3	.199+3	.228+3	.310+3	.392+3	.468+3	.446+3	.325+3	.150+3	.492+2
-11	.890+2	.190+3	.218+3	.298+3	.380+3	.458+3	.441+3	.322+3	.149+3	.491+2
-10	.709+2	.173+3	.199+3	.277+3	.357+3	.438+3	.426+3	.317+3	.146+3	.488+2
-9	.506+2	.134+3	.157+3	.228+3	.303+3	.388+3	.387+3	.302+3	.144+3	.480+2
-8	.278+2	.770+2	.934+2	.147+3	.208+3	.293+3	.308+3	.266+3	.135+3	.460+2
-7	.114+2	.323+2	.407+2	.708+2	.109+3	.175+3	.199+3	.203+3	.115+3	.410+2
	TORR=10.									
ADB	.610+2	.340+2	.394+2	.740+2	.121+3	.205+3	.236+3	.251+3	.139+3	.475+2
-11	.290+2	.326+2	.380+2	.721+2	.118+3	.202+3	.233+3	.249+3	.139+3	.474+2
-10	.168+2	.300+2	.353+2	.684+2	.114+3	.196+3	.228+3	.246+3	.138+3	.472+2
-9	.975+1	.239+2	.288+2	.590+2	.101+3	.181+3	.214+3	.238+3	.135+3	.465+2
-8	.502+1	.142+2	.181+2	.415+2	.759+2	.147+3	.182+3	.216+3	.126+3	.447+2
-7	.204+1	.611+1	.821+1	.219+2	.437+2	.962+2	.127+3	.171+3	.110+3	.401+2

Table V.6. Normalized Thermal Response from X-Rays in Copper with Xenon Gas Protection

Surface Temperature Rise
[°C per J/cm^2]
(Gas at 273 °K)

log Δt (sec)	BLACKBODY TEMPERATURE (KEV) .1	.2	.3	.4	.5	.75	1.	2.	5.	10.
	TORR=0.									
ADB	.248+5	.139+5	.116+5	.905+4	.741+4	.426+4	.285+4	.800+3	.193+3	.553+2
-11	.183+5	.115+5	.997+4	.798+4	.660+4	.389+4	.261+4	.764+3	.190+3	.549+2
-10	.122+5	.868+4	.778+4	.644+4	.541+4	.332+4	.225+4	.705+3	.185+3	.541+2
-9	.616+4	.507+4	.474+4	.413+4	.357+4	.236+4	.165+4	.593+3	.173+3	.523+2
-8	.247+4	.226+4	.219+4	.202+4	.183+4	.135+4	.100+4	.443+3	.154+3	.468+2
-7	.859+3	.832+3	.821+3	.790+3	.749+3	.622+3	.507+3	.291+3	.125+3	.427+2
	TORR=.1									
ADB	.737+4	.401+4	.331+4	.291+4	.261+4	.186+4	.135+4	.529+3	.167+3	.515+2
-11	.583+4	.340+4	.291+4	.262+4	.240+4	.174+4	.128+4	.515+3	.165+3	.513+2
-10	.410+4	.261+4	.234+4	.219+4	.206+4	.156+4	.116+4	.490+3	.163+3	.508+2
-9	.217+4	.154+4	.148+4	.149+4	.147+4	.120+4	.938+3	.437+3	.156+3	.496+2
-8	.883+3	.678+3	.708+3	.776+3	.820+3	.759+3	.635+3	.352+3	.142+3	.496+2
-7	.308+3	.246+3	.270+3	.319+3	.362+3	.383+3	.351+3	.244+3	.118+3	.414+2
	TORR=.5									
ADB	.209+3	.125+3	.146+3	.224+3	.300+3	.378+3	.360+3	.259+3	.130+3	.446+2
-11	.174+3	.110+3	.135+3	.214+3	.290+3	.369+3	.354+3	.256+3	.129+3	.445+2
-10	.130+3	.885+2	.118+3	.196+3	.272+3	.353+3	.341+3	.252+3	.128+3	.443+2
-9	.738+2	.553+2	.867+2	.158+3	.229+3	.312+3	.309+3	.239+3	.125+3	.436+2
-8	.314+2	.255+2	.490+2	.102+3	.159+3	.236+3	.245+3	.210+3	.117+3	.418+2
-7	.111+2	.941+1	.210+2	.500+2	.844+2	.140+3	.156+3	.158+3	.100+3	.375+2
	TORR=1.									
ADB	.339+1	.269+1	.125+2	.411+2	.773+2	.136+3	.152+3	.161+3	.107+3	.398+2
-11	.293+1	.243+1	.121+2	.401+2	.759+2	.135+3	.150+3	.159+3	.107+3	.397+2
-10	.228+1	.202+1	.112+2	.363+2	.732+2	.131+3	.146+3	.157+3	.106+3	.395+2
-9	.137+1	.133+1	.930+1	.336+2	.658+2	.121+3	.137+3	.152+3	.104+3	.390+2
-8	.605+0	.644+0	.609+1	.246+2	.506+2	.980+2	.115+3	.137+3	.988+2	.376+2
-7	.218+0	.243+0	.292+1	.135+2	.300+2	.631+2	.780+2	.107+3	.855+2	.341+2
	TORR=5.									
ADB	.510-12	.292-09	.794-3	.963-1	.723+0	.227+1	.375+1	.265+2	.467+2	.232+2
-11	.478-12	.279-09	.780-3	.953-1	.718+0	.225+1	.372+1	.264+2	.466+2	.232+2
-10	.419-12	.255-09	.753-3	.935-1	.708+0	.222+1	.368+1	.262+2	.464+2	.232+2
-9	.299-12	.198-09	.676-3	.881-1	.679+0	.214+1	.355+1	.257+2	.459+2	.230+2
-8	.153-12	.114-09	.507-3	.742-1	.598+0	.190+1	.319+1	.241+2	.443+2	.225+2
-7	.593-13	.474-10	.277-3	.490-1	.434+0	.140+1	.240+1	.203+2	.402+2	.211+2
	TORR=10.									
ADB	.513-27	.599-20	.419-7	.499-3	.194-1	.667-1	.163+0	.768+1	.252+2	.155+2
-11	.484-27	.574-20	.412-7	.495-3	.193-1	.663-1	.162+0	.766+1	.252+2	.155+2
-10	.430-27	.525-20	.399-7	.487-3	.190-1	.656-1	.161+0	.762+1	.251+2	.154+2
-9	.314-27	.410-20	.361-7	.462-3	.184-1	.634-1	.156+0	.750+1	.249+2	.154+2
-8	.166-27	.237-20	.275-7	.398-3	.166-1	.572-1	.141+0	.715+1	.243+2	.151+2
-7	.651-28	.993-21	.153-7	.272-3	.126-1	.434-1	.109+0	.624+1	.227+2	.145+2

Table V.7. Normalized Thermal Response from X-Rays in Molybdenum with Helium Gas Protection

Surface Temperature Rise
[°C per J/cm^2]
(Gas at 273 °K)

log Δt (sec)	BLACKBODY TEMPERATURE (KEV) .1	.2	.3	.4	.5	.75	1.	2.	5.	10.
	TORR=0.									
ADB	.350+5	.262+5	.170+5	.118+5	.880+4	.537+4	.379+4	.137+4	.271+3	.842+2
-11	.290+5	.224+5	.149+5	.106+5	.802+4	.503+4	.361+4	.133+4	.268+3	.839+2
-10	.211+5	.171+5	.119+5	.873+4	.683+4	.450+4	.332+4	.127+4	.262+3	.834+2
-9	.113+5	.990+4	.754+4	.593+4	.492+4	.355+4	.275+4	.113+4	.248+3	.817+2
-8	.468+4	.438+4	.372+4	.321+4	.287+4	.233+4	.192+4	.881+3	.218+3	.778+2
-7	.165+4	.161+4	.149+4	.139+4	.132+4	.119+4	.105+4	.567+3	.173+3	.702+2
	TORR=.1									
ADB	.338+5	.259+5	.169+5	.117+5	.877+4	.536+4	.379+4	.137+4	.271+3	.842+2
-11	.279+5	.221+5	.149+5	.105+5	.799+4	.503+4	.361+4	.133+4	.266+3	.839+2
-10	.203+5	.169+5	.119+5	.870+4	.651+4	.450+4	.332+4	.127+4	.262+3	.834+2
-9	.109+5	.979+4	.750+4	.591+4	.491+4	.355+4	.275+4	.113+4	.248+3	.817+2
-8	.446+4	.433+4	.370+4	.320+4	.286+4	.232+4	.192+4	.881+3	.218+3	.778+2
-7	.157+4	.159+4	.149+4	.139+4	.132+4	.119+4	.105+4	.567+3	.173+3	.702+2
	TORR=.5									
ADB	.316+5	.252+5	.166+5	.116+5	.869+4	.533+4	.377+4	.136+4	.271+3	.842+2
-11	.260+5	.215+5	.146+5	.104+5	.792+4	.500+4	.360+4	.133+4	.268+3	.839+2
-10	.188+5	.164+5	.117+5	.860+4	.676+4	.448+4	.331+4	.126+4	.262+3	.834+2
-9	.995+4	.952+4	.739+4	.585+4	.487+4	.354+4	.275+4	.113+4	.246+3	.817+2
-8	.403+4	.421+4	.365+4	.317+4	.285+4	.232+4	.192+4	.880+3	.218+3	.778+2
-7	.141+4	.155+4	.147+4	.138+4	.132+4	.118+4	.105+4	.567+3	.173+3	.702+2
	TORR=1.									
ADB	.297+5	.245+5	.163+5	.114+5	.859+4	.529+4	.376+4	.136+4	.271+3	.842+2
-11	.244+5	.209+5	.143+5	.102+5	.784+4	.497+4	.358+4	.133+4	.266+3	.839+2
-10	.176+5	.160+5	.115+5	.849+4	.670+4	.445+4	.330+4	.126+4	.262+3	.834+2
-9	.923+4	.927+4	.728+4	.579+4	.484+4	.353+4	.274+4	.112+4	.247+3	.817+2
-8	.370+4	.410+4	.360+4	.315+4	.283+4	.231+4	.192+4	.880+3	.218+3	.777+2
-7	.129+4	.151+4	.145+4	.137+4	.131+4	.118+4	.105+4	.567+3	.173+3	.702+2
	TORR=5.									
ADB	.206+5	.204+5	.144+5	.104+5	.798+4	.507+4	.365+4	.135+4	.271+3	.842+2
-11	.169+5	.175+5	.127+5	.938+4	.733+4	.478+4	.349+4	.131+4	.266+3	.839+2
-10	.121+5	.135+5	.103+5	.786+4	.633+4	.432+4	.323+4	.125+4	.262+3	.833+2
-9	.632+4	.797+4	.665+4	.545+4	.464+4	.345+4	.270+4	.112+4	.247+3	.817+2
-8	.249+4	.357+4	.334+4	.300+4	.274+4	.228+4	.190+4	.877+3	.216+3	.777+2
-7	.852+3	.132+4	.136+4	.132+4	.128+4	.117+4	.104+4	.566+3	.173+3	.701+2
	TORR=10.									
ADB	.147+5	.171+5	.127+5	.948+4	.745+4	.487+4	.356+4	.133+4	.270+3	.842+2
-11	.122+5	.146+5	.114+5	.863+4	.688+4	.461+4	.341+4	.130+4	.267+3	.839+2
-10	.877+4	.116+5	.930+4	.731+4	.599+4	.419+4	.317+4	.124+4	.261+3	.833+2
-9	.461+4	.696+4	.612+4	.515+4	.445+4	.338+4	.267+4	.111+4	.247+3	.817+2
-8	.183+4	.317+4	.312+4	.288+4	.267+4	.225+4	.188+4	.875+3	.216+3	.777+2
-7	.626+3	.118+4	.128+4	.128+4	.125+4	.116+4	.103+4	.565+3	.173+3	.701+2

Table V.8. Normalized Thermal Response from X-Rays in Molybdenum with Neon Gas Protection

Surface Temperature Rise
[°C per J/cm^2]
(Gas at 273 °K)

log Δt (sec)	BLACKBODY TEMPERATURE (KEV)									
	.1	.2	.3	.4	.5	.75	1.	2.	5.	10
	TORR=0.									
ADB	.350+5	.262+5	.170+5	.118+5	.880+4	.537+4	.379+4	.137+4	.271+3	.842+2
-11	.290+5	.224+5	.149+5	.106+5	.802+4	.503+4	.361+4	.133+4	.268+3	.839+2
-10	.211+5	.171+5	.119+5	.873+4	.683+4	.450+4	.332+4	.127+4	.262+3	.834+2
-9	.113+5	.990+4	.754+4	.593+4	.492+4	.355+4	.275+4	.113+4	.248+3	.817+2
-8	.468+4	.438+4	.372+4	.321+4	.287+4	.233+4	.192+4	.881+3	.218+3	.778+2
-7	.165+4	.161+4	.149+4	.139+4	.132+4	.119+4	.105+4	.567+3	.173+3	.702+2
	TORR=.1									
ADB	.255+5	.218+5	.145+5	.102+5	.778+4	.491+4	.355+4	.132+4	.268+3	.839+2
-11	.210+5	.186+5	.127+5	.915+4	.710+4	.462+4	.339+4	.128+4	.265+3	.836+2
-10	.151+5	.142+5	.101+5	.758+4	.607+4	.415+4	.313+4	.122+4	.260+3	.831+2
-9	.794+4	.822+4	.643+4	.517+4	.440+4	.330+4	.261+4	.109+4	.245+3	.815+2
-8	.317+4	.362+4	.317+4	.282+4	.259+4	.218+4	.184+4	.862+3	.216+3	.776+2
-7	.110+4	.133+4	.128+4	.124+4	.121+4	.112+4	.101+4	.558+3	.172+3	.700+2
	TORR=.5									
ADB	.115+5	.126+5	.871+4	.646+4	.527+4	.374+4	.291+4	.118+4	.259+3	.829+2
-11	.950+4	.109+5	.769+4	.583+4	.485+4	.355+4	.279+4	.115+4	.256+3	.827+2
-10	.687+4	.835+4	.618+4	.488+4	.420+4	.323+4	.261+4	.111+4	.251+3	.822+2
-9	.362+4	.487+4	.393+4	.338+4	.311+4	.263+4	.222+4	.101+4	.236+3	.807+2
-8	.144+4	.214+4	.196+4	.188+4	.188+4	.179+4	.160+4	.805+3	.211+3	.769+2
-7	.493+3	.785+3	.801+3	.848+3	.90?+3	.946+3	.899+3	.530+3	.170+3	.697+2
	TORR=1.									
ADB	.575+4	.769+4	.548+4	.427+4	.371+4	.295+4	.245+4	.108+4	.250+3	.819+2
-11	.480+4	.669+4	.486+4	.388+4	.344+4	.282+4	.237+4	.106+4	.247+3	.817+2
-10	.354+4	.521+4	.393+4	.327+4	.301+4	.260+4	.223+4	.102+4	.243+3	.812+2
-9	.192+4	.307+4	.251+4	.229+4	.227+4	.215+4	.192+4	.935+3	.231+3	.798+2
-8	.774+3	.135+4	.125+4	.130+4	.140+4	.150+4	.141+4	.757+3	.206+3	.763+2
-7	.267+3	.494+3	.518+3	.597+3	.688+3	.805+3	.805+3	.505+3	.167+3	.693+2
	TORR=5.									
ADB	.438+3	.918+3	.726+3	.759+3	.923+3	.120+4	.124+4	.744+3	.209+3	.774+2
-11	.349+3	.824+3	.659+3	.708+3	.879+3	.117+4	.122+4	.735+3	.208+3	.772+2
-10	.265+3	.671+3	.549+3	.622+3	.802+3	.111+4	.117+4	.717+3	.205+3	.768+2
-9	.157+3	.417+3	.362+3	.465+3	.647+3	.965+3	.105+4	.670+3	.198+3	.758+2
-8	.677+2	.187+3	.183+3	.280+3	.430+3	.711+3	.809+3	.563+3	.182+3	.730+2
-7	.240+2	.679+2	.760+2	.134+3	.220+3	.402+3	.487+3	.395+3	.152+3	.671+2
	TORR=10.									
ADB	.134+3	.165+3	.138+3	.212+3	.349+3	.632+3	.753+3	.556+3	.183+3	.739+2
-11	.801+2	.149+3	.127+3	.201+3	.337+3	.620+3	.741+3	.551+3	.182+3	.738+2
-10	.517+2	.124+3	.107+3	.182+3	.315+3	.596+3	.718+3	.540+3	.181+3	.735+2
-9	.284+2	.788+2	.731+2	.144+3	.266+3	.533+3	.656+3	.511+3	.176+3	.726+2
-8	.121+2	.359+2	.378+2	.924+3	.185+3	.408+3	.524+3	.441+3	.164+3	.704+2
-7	.430+2	.131+2	.159+2	.453+2	.979+2	.240+3	.330+3	.322+3	.141+3	.653+2

Table V.9. Normalized Thermal Response from X-Rays in Molybdenum with Xenon Gas Protection

Surface Temperature Rise
[°C per J/cm^2]
(Gas at 273 °J)

log Δt (sec)	BLACKBODY TEMPERATURE (KEV) .1	.2	.3	.4	.5	.75	1.	2.	5.	10
	TORR=0.									
ADB	.350+5	.262+5	.170+5	.118+5	.880+4	.537+4	.379+4	.137+4	.271+3	.842+2
-11	.290+5	.224+5	.149+5	.106+5	.802+4	.503+4	.361+4	.133+4	.268+3	.839+2
-10	.211+5	.171+5	.119+5	.873+4	.683+4	.450+4	.332+4	.127+4	.262+3	.834+2
-9	.113+5	.990+4	.754+4	.593+4	.492+4	.355+4	.275+4	.113+4	.248+3	.817+2
-8	.468+4	.438+4	.372+4	.321+4	.287+4	.233+4	.192+4	.881+3	.218+3	.778+2
-7	.165+4	.161+4	.149+4	.139+4	.132+4	.119+4	.105+4	.567+3	.173+3	.702+2
	TORR=.1									
ADB	.140+5	.910+4	.554+4	.395+4	.339+4	.271+4	.229+4	.102+4	.235+3	.801+2
-11	.115+5	.761+4	.477+4	.351+4	.310+4	.258+4	.222+4	.100+4	.233+3	.798+2
-10	.823+4	.560+4	.370+4	.289+4	.268+4	.238+4	.209+4	.968+3	.230+3	.794+2
-9	.429+4	.307+4	.227+4	.201+4	.202+4	.199+4	.181+4	.884+3	.220+3	.780+2
-8	.172+4	.130+4	.113+4	.116+4	.128+4	.141+4	.134+4	.715+3	.197+3	.746+2
-7	.597+3	.471+3	.472+3	.547+3	.641+3	.764+3	.764+3	.475+3	.160+3	.679+2
	TORR=.5									
ADB	.551+3	.387+3	.280+3	.380+3	.575+3	.904+3	.961+3	.562+3	.171+3	.699+2
-11	.452+3	.322+3	.245+3	.356+3	.554+3	.884+3	.943+3	.555+3	.170+3	.698+2
-10	.322+3	.234+3	.196+3	.321+3	.518+3	.847+3	.909+3	.541+3	.168+3	.695+2
-9	.165+3	.125+3	.130+3	.259+3	.443+3	.753+3	.820+3	.503+3	.163+3	.686+2
-8	.646+2	.511+2	.733+2	.176+3	.317+3	.564+3	.632+3	.418+3	.150+3	.663+2
-7	.221+2	.182+2	.350+2	.917+2	.1·0+3	.319+3	.375+3	.289+3	.127+3	.616+2
	TORR=1.									
ADB	.108+2	.890+1	.204+2	.926+2	.203+3	.412+3	.474+3	.319+3	.129+3	.624+2
-11	.892+1	.747+1	.193+2	.902+2	.199+3	.404+3	.467+3	.315+3	.129+3	.623+2
-10	.639+1	.551+1	.175+2	.858+2	.191+3	.390+3	.452+3	.308+3	.128+3	.621+2
-9	.330+1	.300+1	.142+2	.747+2	.169+3	.351+3	.412+3	.289+3	.125+3	.615+2
-8	.129+1	.126+1	.966+1	.532+2	.124+3	.268+3	.323+3	.245+3	.117+3	.600+2
-7	.438+0	.462+0	.501+1	.278+2	.676+2	.154+3	.196+3	.175+3	.103+3	.565+2
	TORR=5.									
ADB	.237-11	.165-09	.242-2	.334+0	.256+1	.804+1	.116+2	.198+2	.544+2	.430+2
-11	.204-11	.162-09	.236-2	.328+0	.252+1	.794+1	.115+2	.197+2	.543+2	.430+2
-10	.155-11	.157-09	.223-2	.318+0	.246+1	.776+1	.112+2	.196+2	.542+2	.430+2
-9	.867-12	.144-09	.190-2	.287+0	.228+1	.723+1	.105+2	.191+2	.539+2	.428+2
-8	.354-12	.114-09	.127-2	.218+0	.185+1	.593+1	.879+1	.178+2	.530+2	.423+2
-7	.122-12	.672-10	.609-3	.122+0	.115+1	.374+1	.581+1	.154+2	.506+2	.409+2
	TORR=10.									
ADB	.244-26	.332-20	.136-6	.175-2	.690-1	.238+0	.390+0	.378+1	.374+2	.341+2
-11	.213-26	.327-20	.133-6	.172-2	.683-1	.236+0	.386+0	.377+1	.374+2	.341+2
-10	.165-26	.319-20	.126-6	.167-2	.670-1	.231+0	.380+0	.376+1	.373+2	.340+2
-9	.937-27	.294-20	.107-6	.153-2	.629-1	.217+0	.360+0	.374+1	.372+2	.339+2
-8	.388-27	.235-20	.720-7	.119-2	.527-1	.182+0	.309+0	.366+1	.367+2	.336+2
-7	.135-27	.140-20	.344-7	.689-3	.343-1	.119+0	.215+0	.347+1	.353+2	.326+2

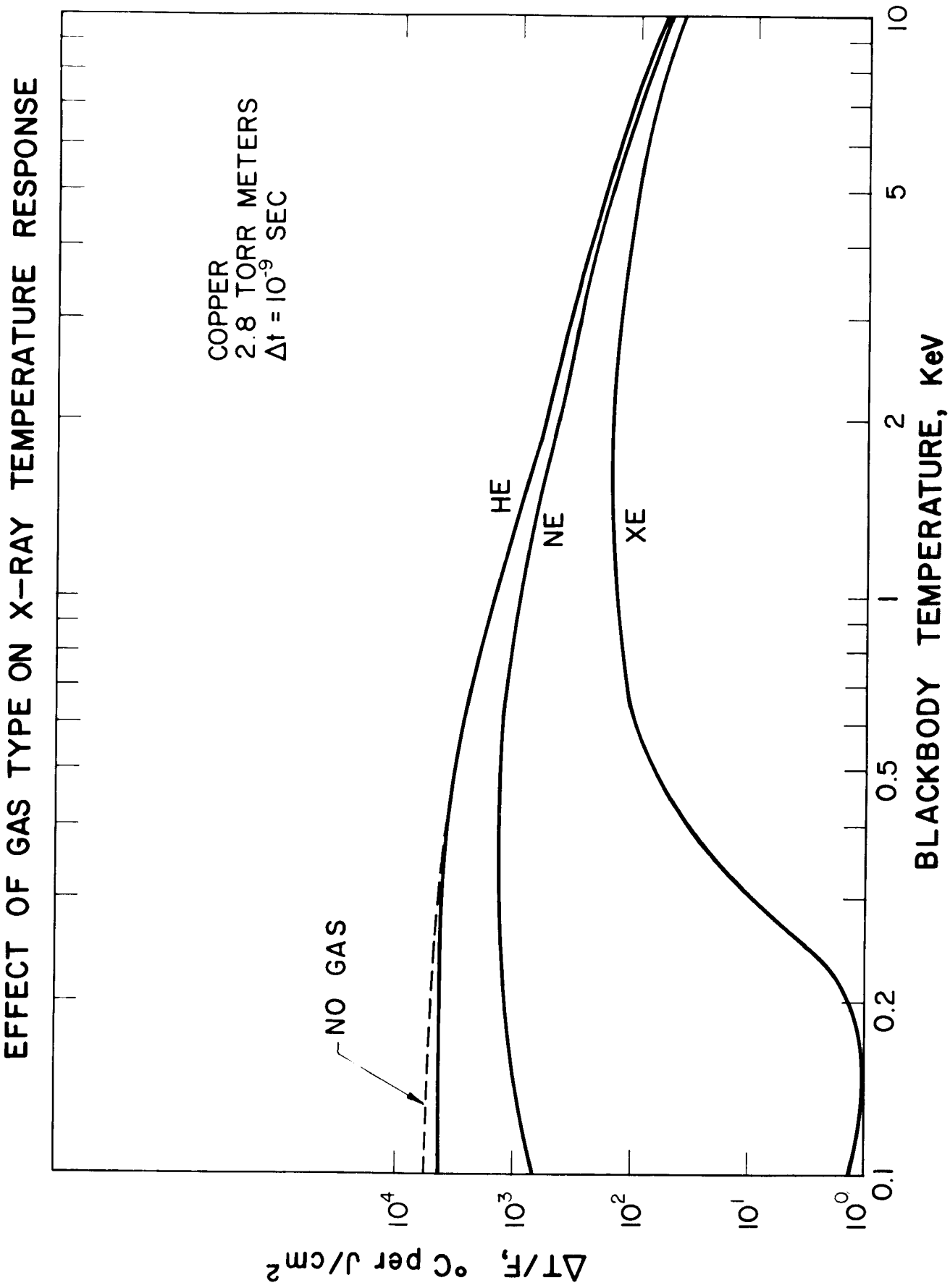
EFFECT OF GAS TYPE ON X-RAY TEMPERATURE RESPONSE
COPPER
2.8 TORR METERS
Δt = 10⁻⁹ SEC
NO GAS
HE
NE
XE
ΔT/F, °C per J/cm²
BLACKBODY TEMPERATURE, KeV
0.1
0.2
0.5
1
2
5
10
10⁰
10¹
10²
10³
10⁴

FIGURE 16

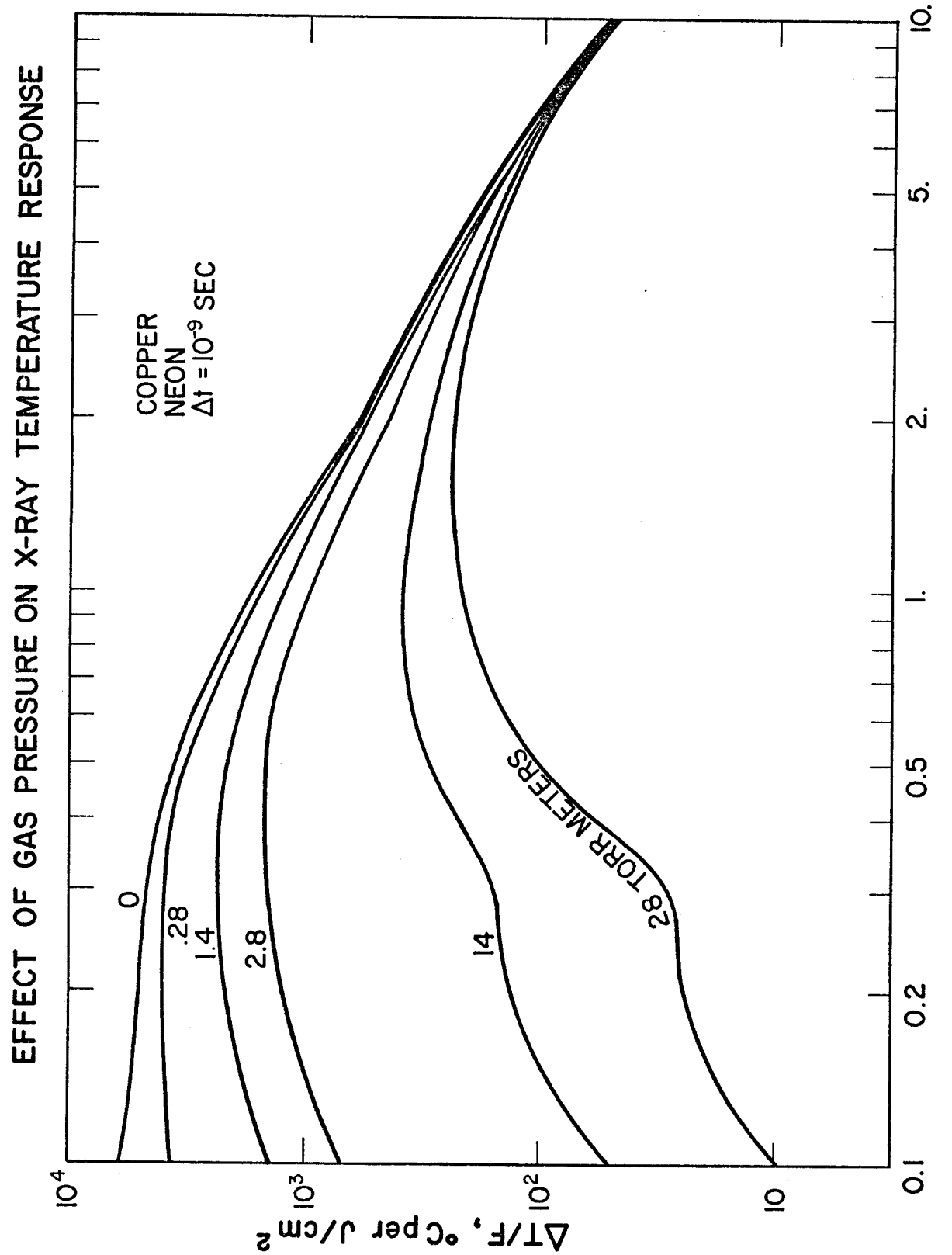
EFFECT OF GAS PRESSURE ON X-RAY TEMPERATURE RESPONSE
COPPER
NEON
Δt = 10⁻⁹ SEC
0
.28
1.4
2.8
14
28 TORR METERS
ΔT/F, °C per J/cm²
10⁴
10³
10²
10
0.1
0.2
0.5
1.
2.
5.
10.
BLACK BODY TEMPERATURE, KeV

FIGURE 17

FIGURE 18

EFFECT OF SOURCE TIME ON X-RAY TEMPERATURE RESPONSE

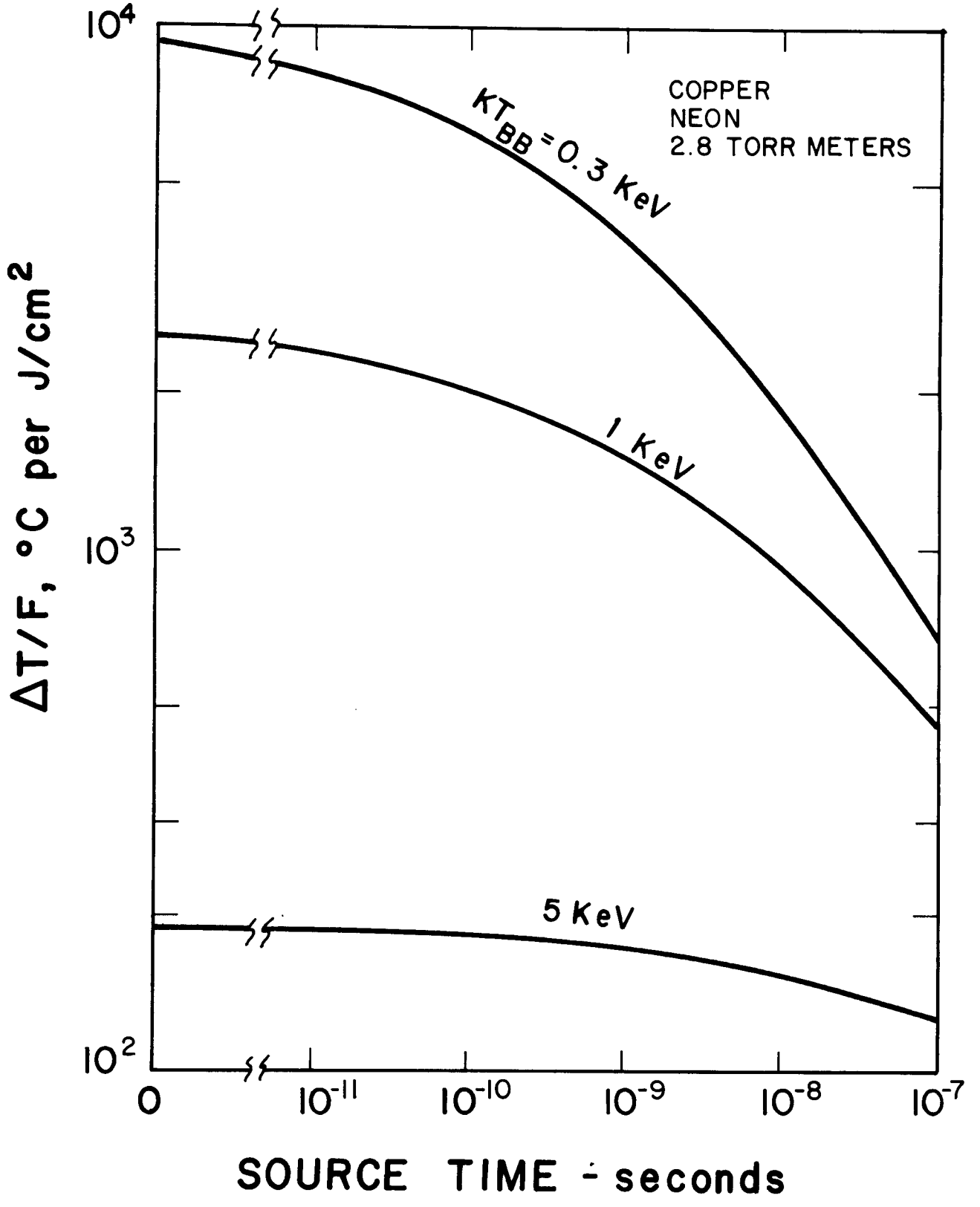

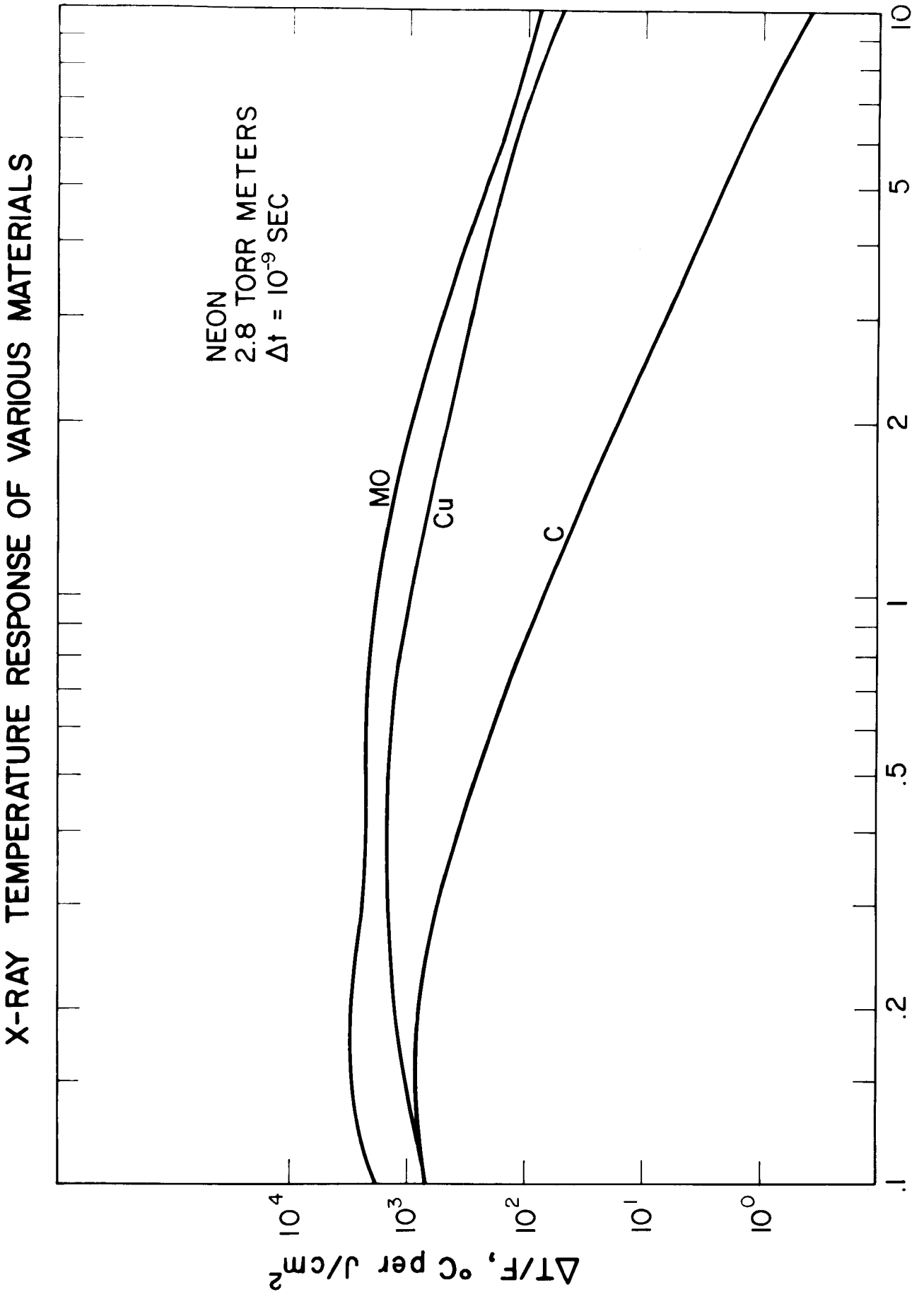
X-RAY TEMPERATURE RESPONSE OF VARIOUS MATERIALS
NEON
2.8 TORR METERS
Δt = 10⁻⁹ SEC
Mo
Cu
C
ΔT/F, °C per J/cm²
BLACKBODY TEMPERATURE, KeV
10⁴
10³
10²
10¹
10⁰
.1
.2
.5
1
2
5
10

FIGURE 19

V.B. Effect on General Ion and Photon Spectra

V.B.1. Single Heavy Ion Spectrum

In this section the effect of a gaseous layer on wall response is demonstrated for general spectra. The first example is characteristic of an output spectrum which is dominated by a single heavy ion. The heavy ion chosen is mercury with a total energy of 14.8 MJ and an initial gaussian spectrum of 3 ± 1 MeV. The response is analyzed for a molybdenum wall at a radius of 6 meters with a protective layer of neon gas. This spectrum is typical of that expected from a heavily structured pellet calculation. The entire bare wall response to this spectrum was reported in reference 16 and only the comparison for the heavy ion component with gaseous protection is given here.

The mercury induced temperature excursion in the molybdenum for various gas pressures is shown in figure 20. These data indicate that pressures as low as a few tenths of a torr (0.6-2.0 torr-meters) are sufficient to reduce the temperature rise considerably. The thermal response is reduced until ~0.4 torr of Ne gas finally absorbs all the ions' energy and no mercury ions reach the wall.

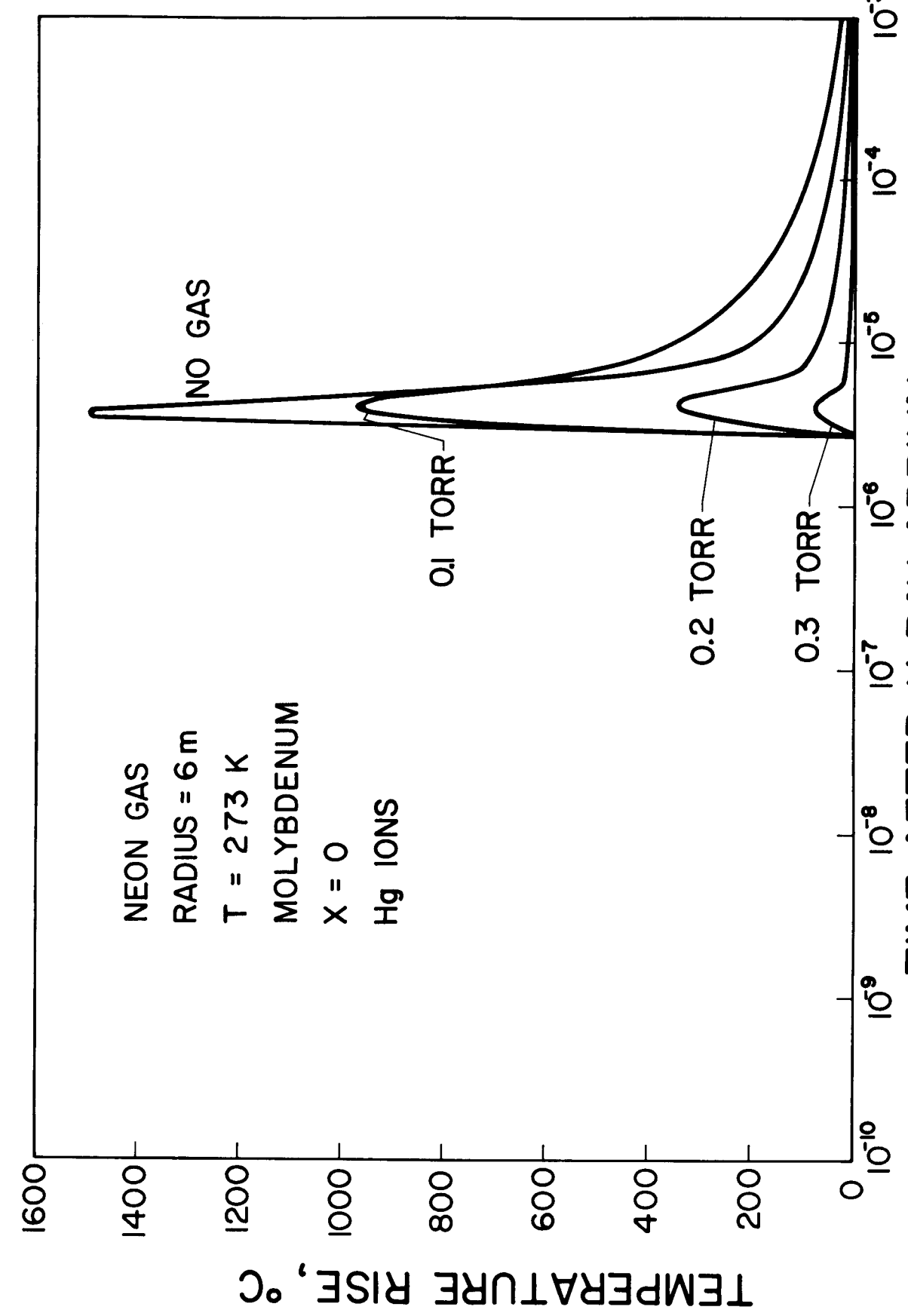
EFFECT OF GAS PRESSURE ON TEMPERATURE RESPONSE
NEON GAS
RADIUS = 6 m
T = 273 K
MOLYBDENUM
X = 0
Hg IONS
NO GAS
0.1 TORR
0.2 TORR
0.3 TORR
TEMPERATURE RISE, °C
TIME AFTER X-RAY ARRIVAL, sec
1600
1400
1200
1000
800
600
400
200
0
10^{-10}
10^{-9}
10^{-8}
10^{-7}
10^{-6}
10^{-5}
10^{-4}
10^{-3}

FIGURE 20

V.B.2. Response to a General Spectrum

As a reference spectrum for a general comparison of the effect of gas protection we have chosen that originally given in reference 2 (table V.10). This spectrum contains both light and heavy ions as well as X-rays and reflected laser light. The T*DAMEN code, using the methodology in previous chapters, was used to calculate the response of a copper surface at 7 meters.

The effect of 0.5 torr of neon on each of the components is demonstrated in the spectra shown in figure 21. Each component is shifted down in energy and the spectra is broadened as the ions' energy is reduced. The most notable shift is in the silicon ions in which many of the lower energy ions do not penetrate the gas. The modification of the X-ray spectrum shows the high absorption near the K-edge of neon.

The flux and arrival times associated with each species are depicted in figure 22. Each pulse is lowered in peak amplitude and spread in time by the gas. The silicon component, however, is noted to not only be reduced in magnitude but shortened in time since the ions which would normally arrive at late times do not reach the exposed surface. The deuterium and tritium flux were originally the same without gas protection; yet, because of the different stopping powers in neon, the deuterium was more radically modified than the tritium.

The modified spatial energy deposition profiles of the ions are shown in figure 23. The gas is actually observed to increase the surface deposition due to the high energy helium since the ions' energies are moved closer to the peak in the stopping power curves. These less energetic ions, however, do not penetrate as deeply as the original spectrum and the extent of the deposition is reduced. The silicon deposition is the most radically affected due

to the large loss of energy in the gas. These modified energy depositions are coupled with the reduced fluxes of figure 22 to produce a lower temperature rise in the copper.

The total temperature excursions from all of the components are compared in figure 24 and 25. A reduction of about 50% is noted in the temperature transient at the surface with a similiar reduction at a depth of 1 micron. The responses to both ions and photons show a similar reduction at the front surface. At the 1 micron position the temperature excursion is not so significantly reduced since the initial transient is due to higher energy photons which can pass through the gas more easily. The reduction in temperature noted here not only reduces the probability of approaching the melting temperature but also can substantially reduce the severity of other effects such as generation of stress waves, sputtering,[17] and evaporation.

The displacement production at the front surface shows only about a 30% reduction with the gas introduced (figure 26). This is primarily due to the fact that, although the energy and number of silicon ions are reduced, the lower ion energies are characterized by significantly higher effective displacement cross sections. At greater depth, such as at 1 micron in figure 27, the significant reduction of damage is apparent since the silicon ions are less energetic after passing through the gas and do not penetrate to this position. The displacement production by the neutrons is essentially uniform throughout the material and at greater depths (>10 microns) is the only contributor to the displacement rate. The damage at this position is almost entirely produced by the light ion components. The most revealing comparison of the displacement production is given in figure 28 which shows the composite

spatial distribution of all the ion components after the deposition pulse. The peak damage is reduced from 1.2×10^{-3} dpa per pulse to about 3.6×10^{-4} dpa per pulse by the addition of the gas.

Table V.10

Reference Spectra (100 MJ)

	Energy (MJ)	Spectrum
Laser	.2	10.6 μ
X-ray	2	1.0 keV - BB
D	4.6	160 keV - M
T	6.9	240 keV - M
He (Slow)	1.2	320 keV - M
He (Fast)	5.4	2 ± .5 MeV - G
Silicon	2.7	800 keV - M
Neutrons	77.	14 ± 1 MeV - G

BB = Black Body M = Maxwellian G = Gaussian

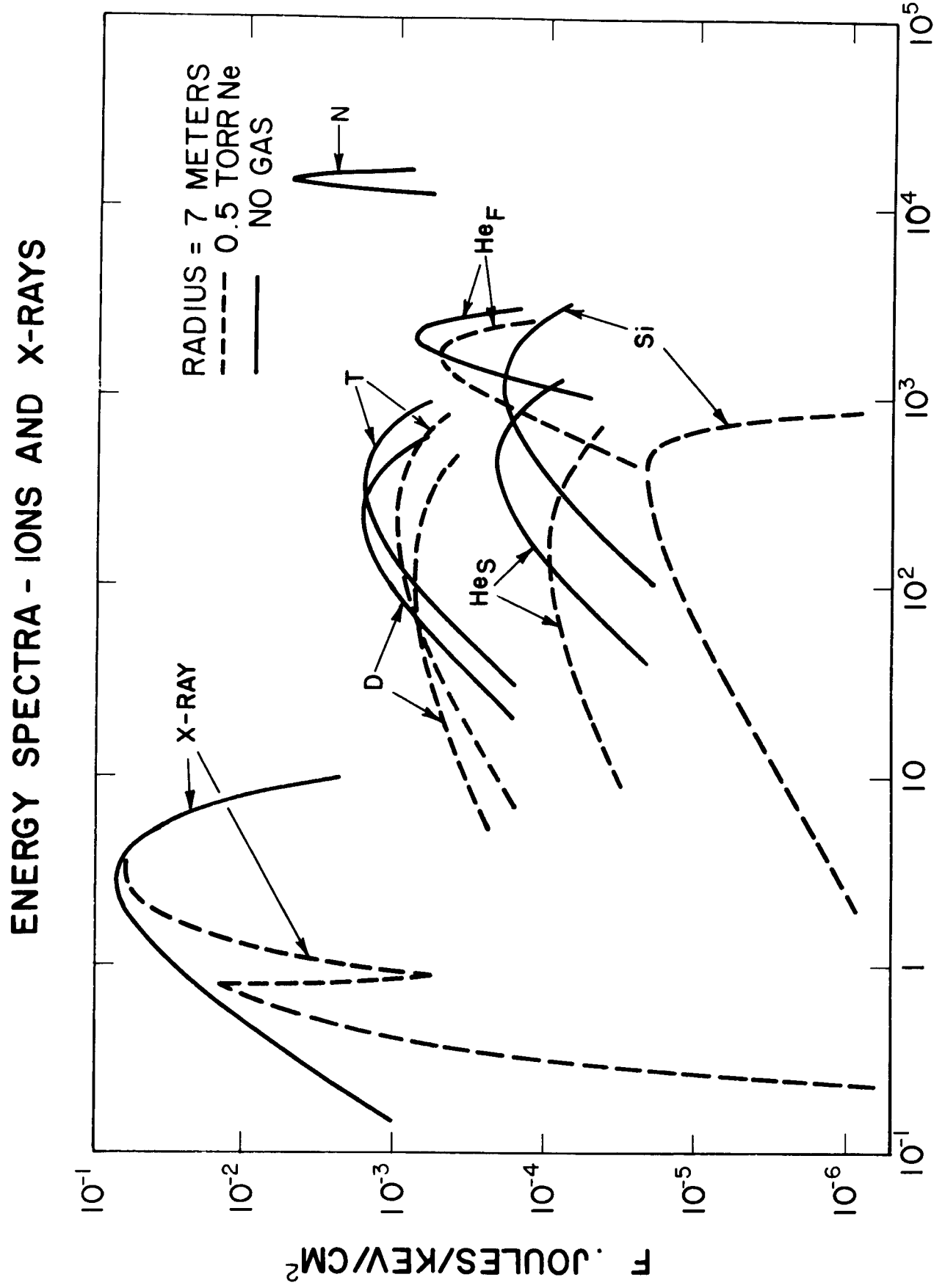
ENERGY SPECTRA - IONS AND X-RAYS
RADIUS = 7 METERS
0.5 TORR Ne
NO GAS
N
X-RAY
D
T
He S
He F
Si
F , JOULES/KEV/CM²
ENERGY, KEV
10⁻¹
10⁻²
10⁻³
10⁻⁴
10⁻⁵
10⁻⁶
1
10
10²
10³
10⁴
10⁵

FIGURE 21

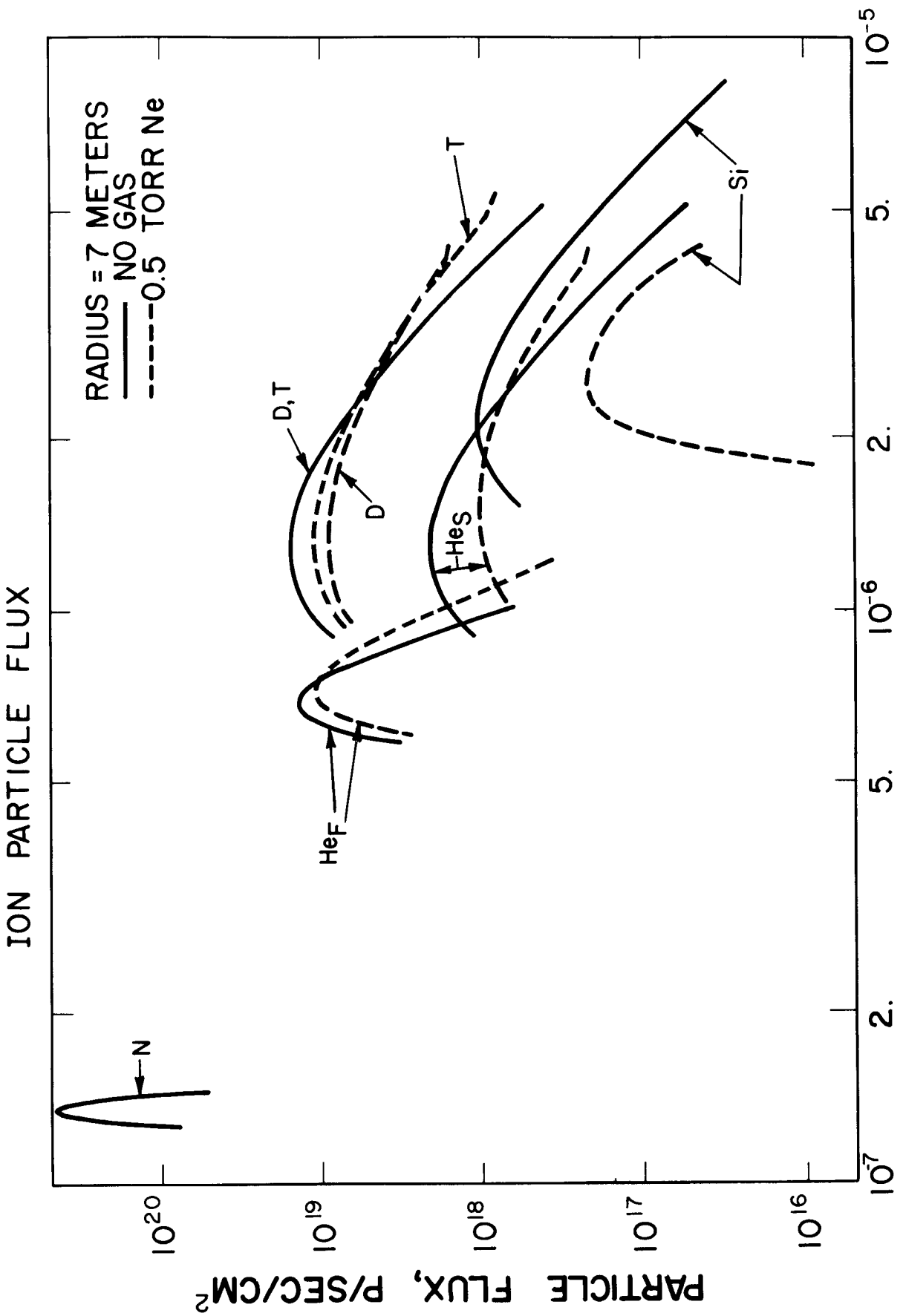
ION PARTICLE FLUX
RADIUS = 7 METERS
NO GAS
0.5 TORR Ne
N
D,T
D
T
He_F
He_S
Si
PARTICLE FLUX, P/SEC/CM²
TIME, SEC
10²⁰
10¹⁹
10¹⁸
10¹⁷
10¹⁶
10⁻⁷
2.
5.
10⁻⁶
2.
5.
10⁻⁵

FIGURE 22

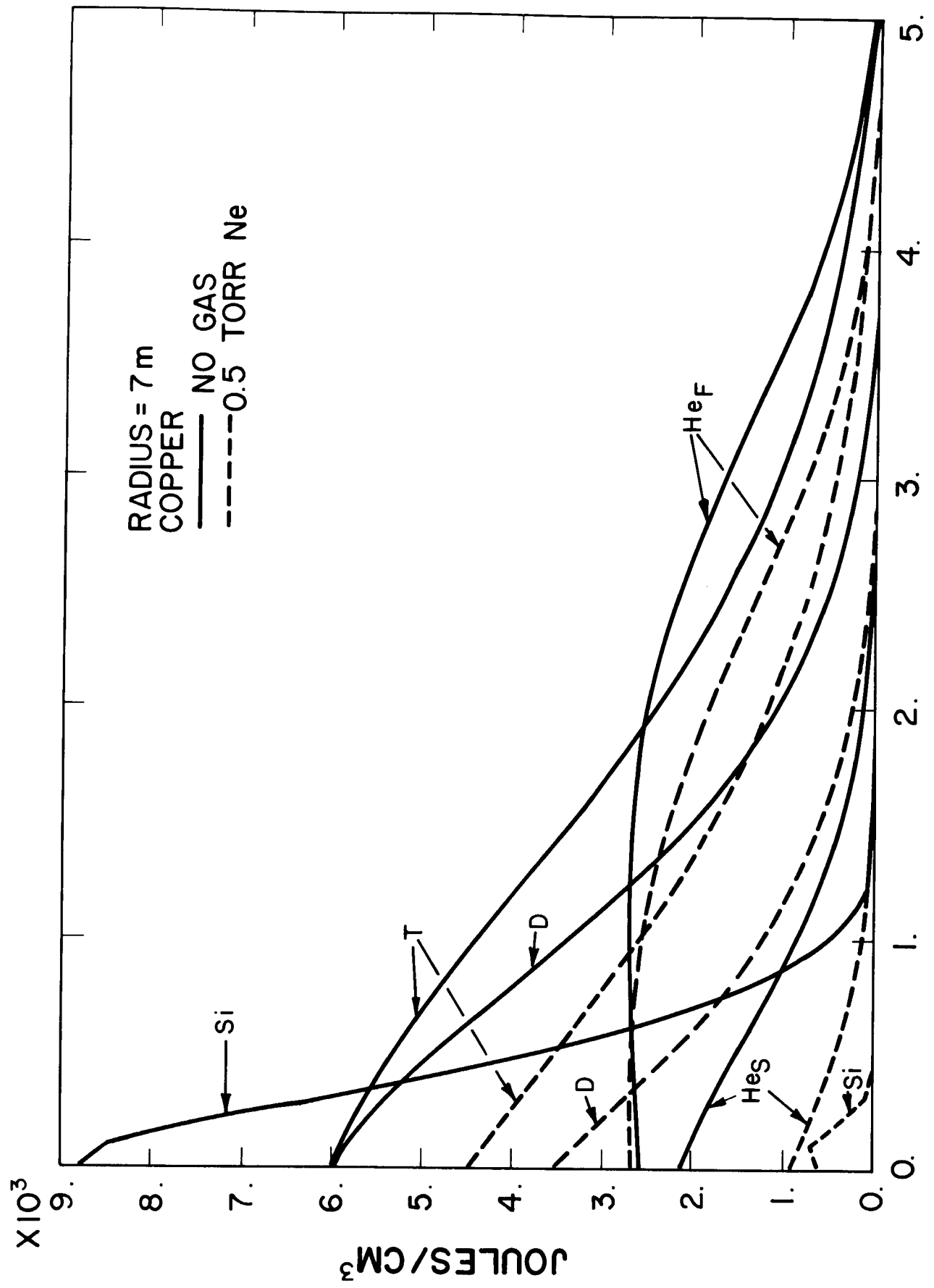
TOTAL DEPOSITED ENERGY
RADIUS = 7 m
COPPER
NO GAS
0.5 TORR Ne
Si
T
D
D
He_F
He$_S$
Si
JOULES/CM^3
X10^3
9.
8.
7.
6.
5.
4.
3.
2.
1.
0.
0.
1.
2.
3.
4.
5.
LOCATION, MICRON

FIGURE 23

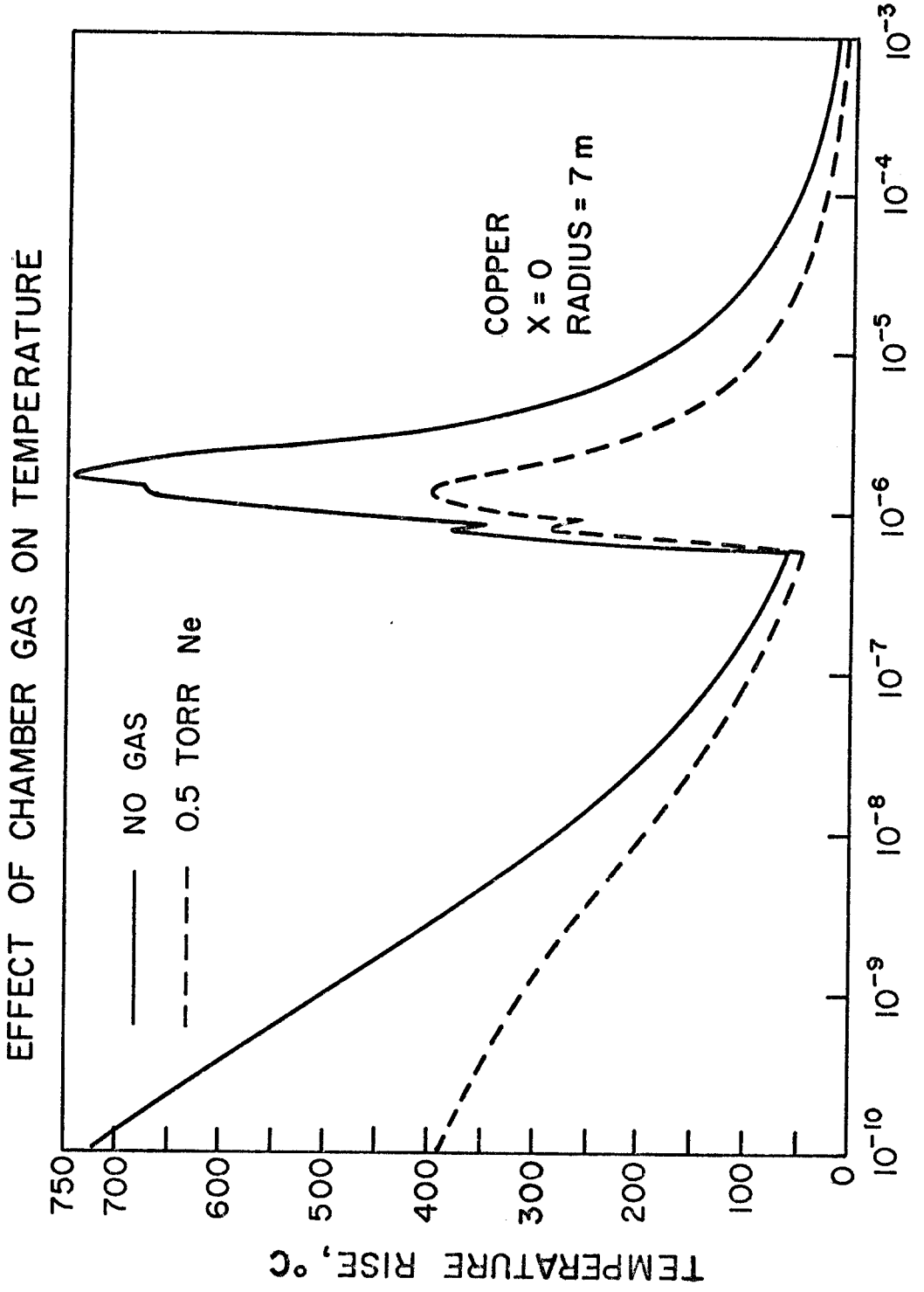
EFFECT OF CHAMBER GAS ON TEMPERATURE
NO GAS
0.5 TORR Ne
COPPER
X = 0
RADIUS = 7 m
TEMPERATURE RISE, °C
TIME AFTER X-RAY ARRIVAL, SEC.
750
700
600
500
400
300
200
100
0
10^{-10}
10^{-9}
10^{-8}
10^{-7}
10^{-6}
10^{-5}
10^{-4}
10^{-3}

FIGURE 24

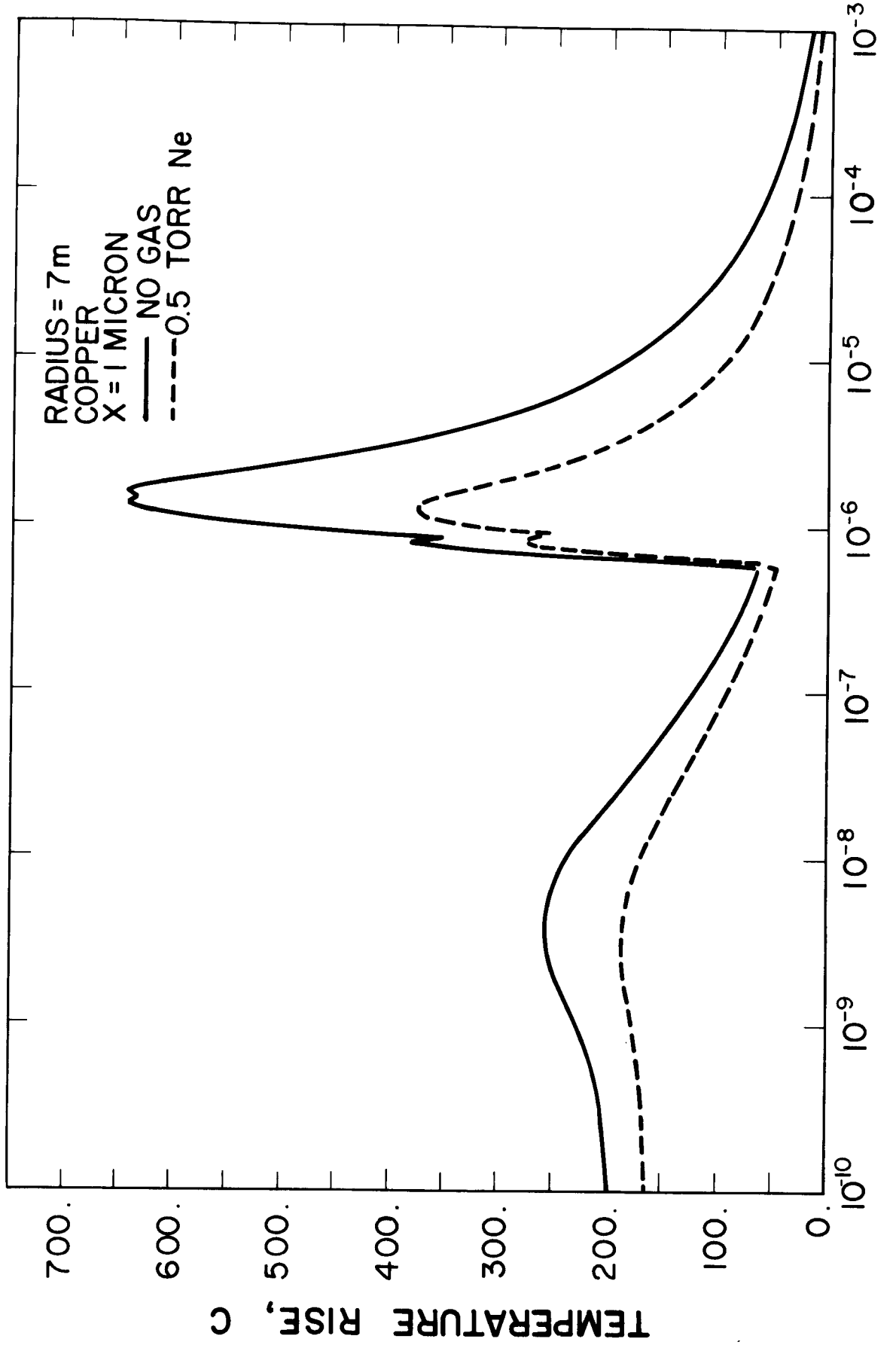
TOTAL TEMPERATURE RESPONSE
RADIUS = 7m
COPPER
X = 1 MICRON
NO GAS
0.5 TORR Ne
TEMPERATURE RISE, C
700.
600.
500.
400.
300.
200.
100.
0.
10^{-10}
10^{-9}
10^{-8}
10^{-7}
10^{-6}
10^{-5}
10^{-4}
10^{-3}
TIME AFTER X-RAY ARRIVAL, sec

FIGURE 25

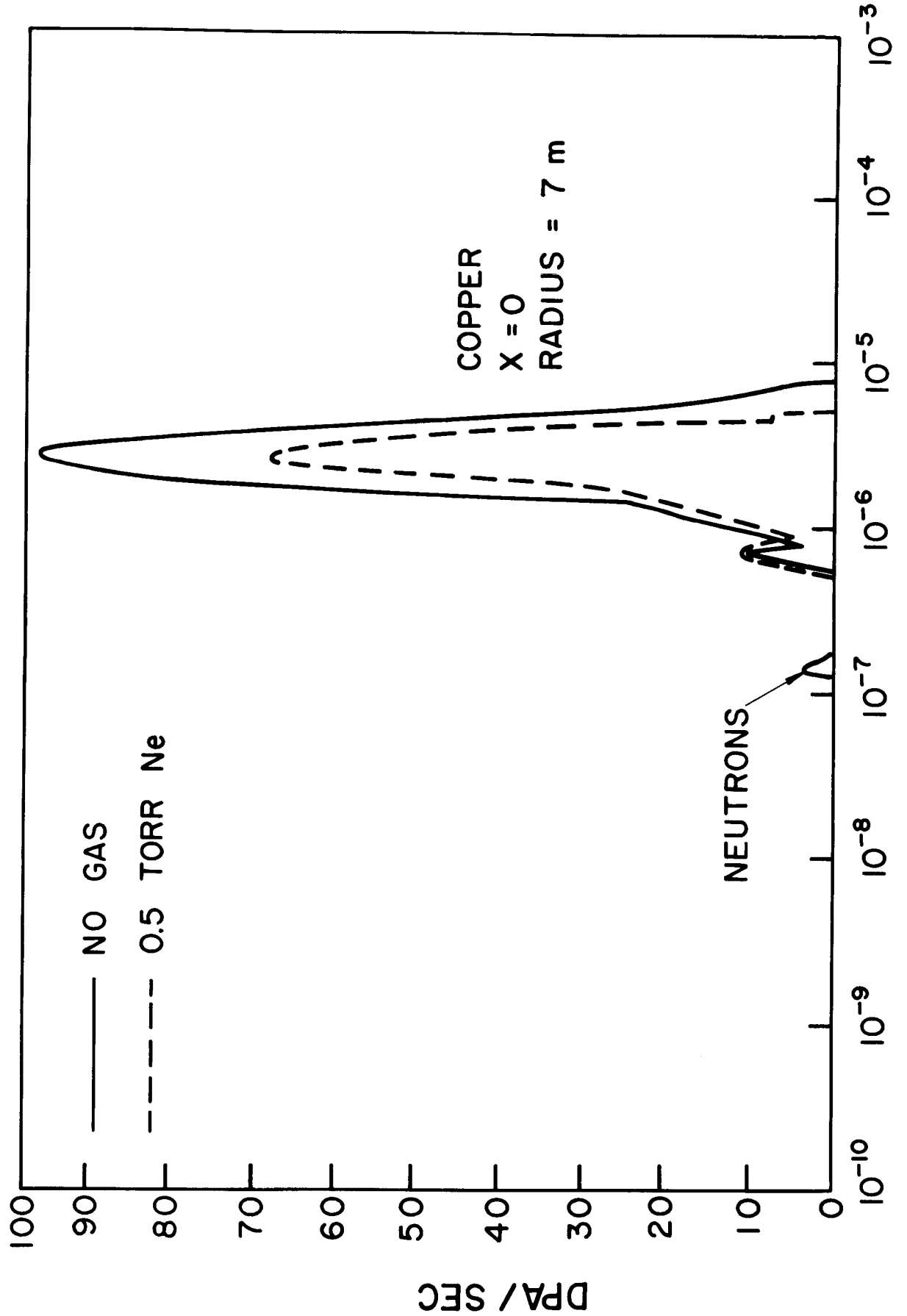
EFFECT OF CHAMBER GAS ON DPA RATE
NO GAS
0.5 TORR Ne
COPPER
X = 0
RADIUS = 7 m
NEUTRONS
DPA / SEC
TIME AFTER X-RAY ARRIVAL, SEC.
100
90
80
70
60
50
40
30
20
10
0
10^{-10}
10^{-9}
10^{-8}
10^{-7}
10^{-6}
10^{-5}
10^{-4}
10^{-3}

FIGURE 26

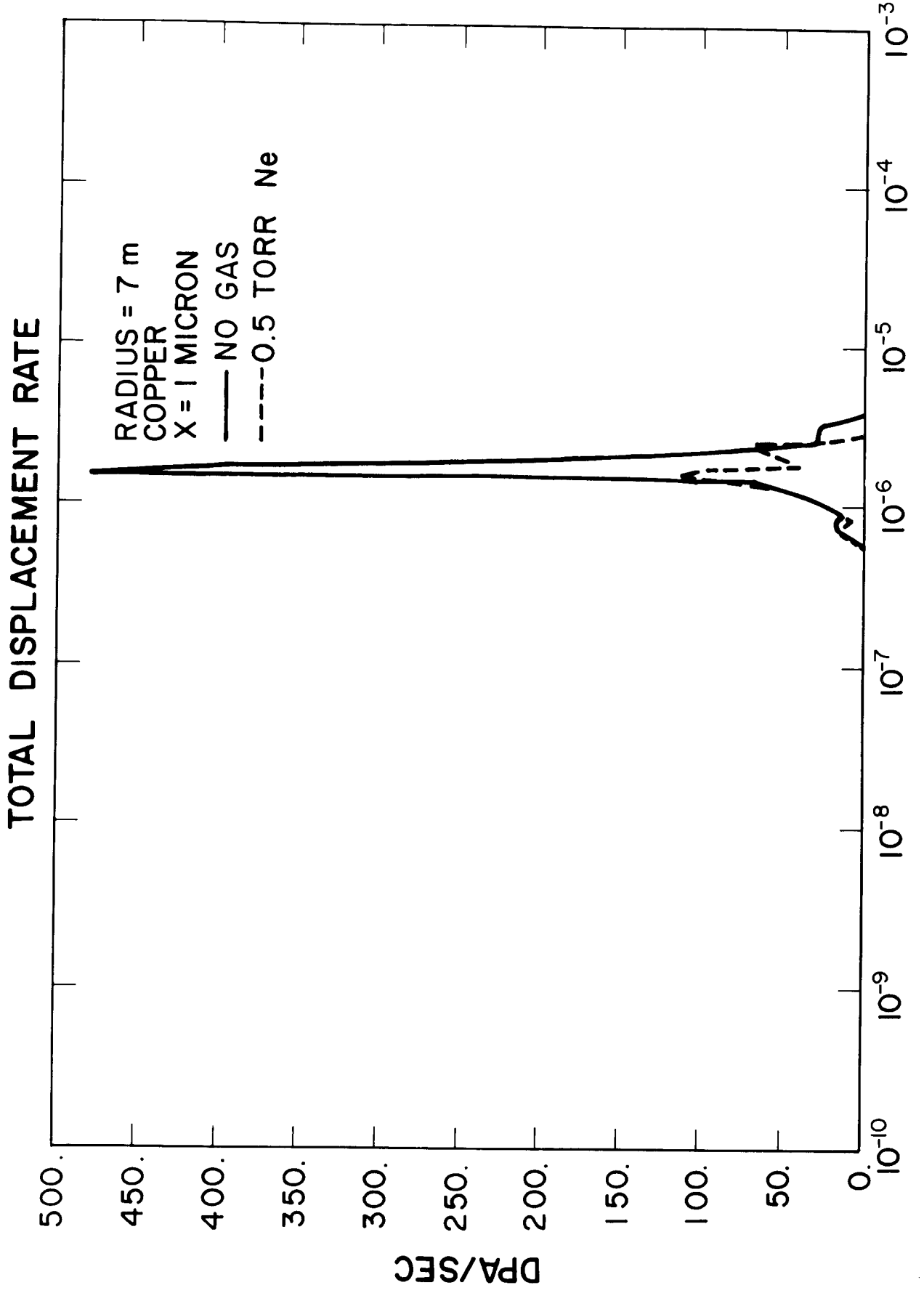
TOTAL DISPLACEMENT RATE
RADIUS = 7 m
COPPER
X = 1 MICRON
NO GAS
0.5 TORR Ne
DPA/SEC
TIME , sec
500.
450.
400.
350.
300.
250.
200.
150.
100.
50.
0.
10^{-10}
10^{-9}
10^{-8}
10^{-7}
10^{-6}
10^{-5}
10^{-4}
10^{-3}

FIGURE 27

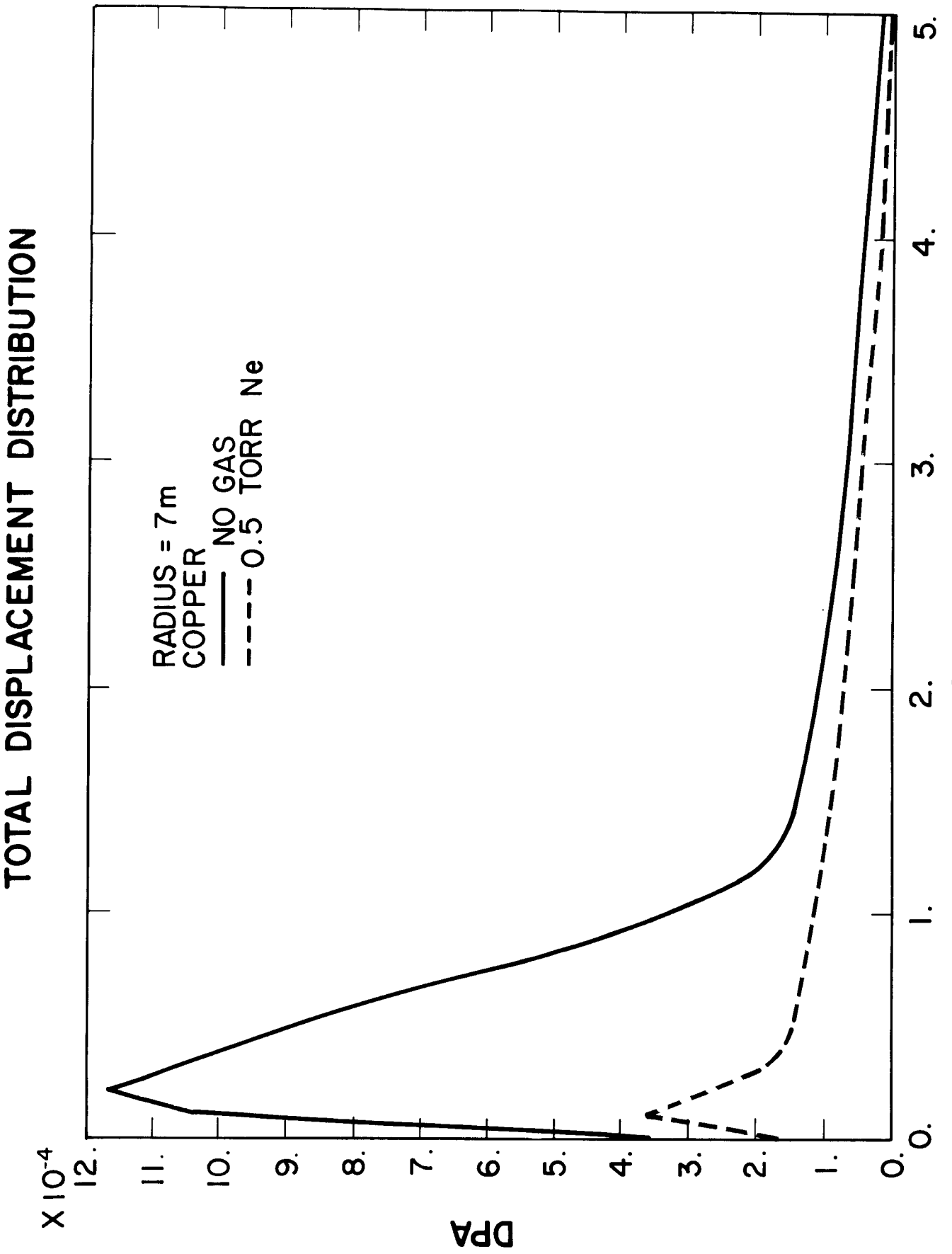
TOTAL DISPLACEMENT DISTRIBUTION
RADIUS = 7m
COPPER
NO GAS
0.5 TORR Ne
DPA
X 10^-4
12.
11.
10.
9.
8.
7.
6.
5.
4.
3.
2.
1.
0.
0.
1.
2.
3.
4.
5.
LOCATION, micron

FIGURE 28

VI. Summary and Conclusions

This document has summarized the effects of gaseous protection on the prompt response of materials exposed to transient thermonuclear radiation. Data indicates that gas pressures in the chamber of an inertial confinement reactor of 0.1 to 10 torr can substantially modify the resultant damage to the first wall.

A diffusion theory for estimating ion distributions at intermediate energies was developed and shown to give reasonable results when compared to more formal theories. General models were thus developed to predict the flux and modified spectra at arbitrary positions in a gas for various gas pressures. These models were incorporated into the T*DAMEN computer code for application to both light and heavy ion spectra.

Application of the models to a variety of photon and ion spectra showed that gas pressures of a few torr can substantially reduce the prompt surface temperature response from photons. For ion spectra, reductions of a factor of two in surface temperature response are noted even for gas pressures which do not stop all the ions in the output spectra. Displacement damage was shown to be significantly reduced by gas layers even though surface damage production is not reduced as much at depths of .5 to 1 micron. Finally, the generality of the models developed allows efficient, yet accurate, assessment of the response of surfaces to a wide range of photon and ion spectra.

VII. Acknowledgement

The authors would like to thank the Department of Energy for partial support of this work.

References

1. Hunter, T.O., and Kulcinski, G.L., UWDFM-196, Nuclear Engineering Department, University of Wisconsin-Madison, March 1977.

2. Hunter, T.O., and Kulcinski, G.L., UWFDM-217, Nuclear Engineering Department, University of Wisconsin-Madison, October 1977.

3. Frank, T., et al., Proceedings of the 1st Topical Mtg on Technology of Controlled Nuclear Fusion, San Diego, CA, April 1974, p. 83.

4. Maniscalco, J.A., et al., Trans Am. Nucl. Soc., 27, 34, (1977).

5. Conn, R.W., et al., UWFDM-220, Vol. I & II, Nuclear Engineering Department, University of Wisconsin-Madison, December 1977.

6. Brice, D.K., SAND75-0622, Sandia Laboratories, Albuquerque, New Mexico, July 1977.

7. Lindhard, J., et al., Mat Fys. Medd. Dar. Vid. Selsk., 33, No. 14, 1963.

8. "Projected Range Statistics", Gibbons, J.F., Johnson, W.S., and Mylroie, S.W.; Halstad Press, 2nd Ed.

9. "Ion Implantation Range and Energy Deposition Distributions", Vol. 2, Winterbon, K.B.; IFI/Plenum, New York, 1975.

10. Brice, D.K., Radiation Effects, 1971, Vol. II, p. 227.

11. Tsurushima, T., and Tanoue H., J. of Physical Soc. of Japan, Vol. 31, No. 6, December 1971.

12. Manning, I., and Mueller, G.P., Computer Physics Communication, 6, 1973.

13. "Mathematical Handbook for Scientists and Engineers", Korn, G.A., and Korn, T.M., McGraw-Hill, 1961.

14. Moses, G., and Smatlak, D., Nuclear Engineering Department, University of Wisconsin-Madison, to be published.

15. Biggs, F., and Lighthill, R., Analytical Approximation for X-ray Cross Sections II, SC-RR-71-0507, Sandia Labs., Albuquerque, N. Mex., December 1971.

16. Hunter, T.O., et al., UWFDM-221, Nuclear Engineering Department, University of Wisconsin-Madison, October 1977.

17. Hunter, T.O., and Kulcinski, G.L., UWFDM-233, Nuclear Engineering Department, University of Wisconsin-Madison, October 1977.